

1
2
3
4
5
6
7 **Application of Immobilized ATP to the Study of NLRP Inflammasomes**
8
9

10
11 Kuo-Chieh Liao^{1,2,#}, Christina F. Sandall^{1,#}, David A. Carlson³, Annegret
12 Ulke-Lemée¹, Jaye M. Platnich², Philip F. Hughes³, Daniel A. Muruve²,
13 Timothy A.J. Haystead³, and Justin A. MacDonald^{1,*}
14

15
16
17 ¹Department of Biochemistry & Molecular Biology, University of Calgary,
18 3280 Hospital Drive NW, Calgary, AB, T2N 4Z6, Canada
19

20
21 ²Department of Medicine, University of Calgary, 3280 Hospital Drive NW,
22 Calgary, AB, T2N 4Z6, Canada

23
24 ³Department of Pharmacology & Cancer Biology, Center for Chemical Biology, Duke
25 University School of Medicine, Box 3813, 450 Research Drive, Durham, NC, 27710, USA
26
27
28
29

30 #- Contributed equally to the manuscript
31

32 \$- Current location: Programme in Emerging Infectious Diseases, Duke-NUS Medical School,
33 Singapore.
34

35 *To whom correspondence should be addressed: Department of Biochemistry & Molecular
36 Biology, University of Calgary, 3280 Hospital Drive NW, Calgary, AB, T2N 4Z6, Canada; E-
37 mail: jmacdo@ucalgary.ca; Tel.: 1-403-210-8433
38
39

40 Key words: nucleotide-binding oligomerization domain, leucine rich repeat and pyrin domain
41 containing-3, NLRP, inflammasome, fluorescence-linked enzyme chemoproteomic strategy,
42 FLECS, selected reaction monitoring mass spectrometry, SRM-MS, immobilized ATP Sepharose,
43 drug discovery
44
45
46
47
48
49
50
51
52
53
54
55
56

57
58
59 **ABSTRACT**
60

61 The NLRP proteins are a subfamily of the NOD-like receptor (NLR) innate immune sensors that
62 possess an ATP-binding NACHT domain. As the most well studied member, NLRP3 can initiate
63 the assembly process of a multiprotein complex, termed the inflammasome, upon detection of a
64 wide range of microbial products and endogenous danger signals and results in the activation of
65 pro-caspase-1, a cysteine protease that regulates multiple host defense pathways including
66 cytokine maturation. Dysregulated NLRP3 activation contributes to inflammation and the
67 pathogenesis of several chronic diseases, and the ATP-binding properties of NLRPs are thought
68 to be critical for inflammasome activation. In light of this, we examined the utility of immobilized
69 ATP matrices in the study of NLRP inflammasomes. Using NLRP3 as the prototypical member of
70 the family, P-linked ATP Sepharose was determined to be a highly-effective capture agent. In
71 subsequent examinations, P-linked ATP Sepharose was used as an enrichment tool to enable the
72 effective profiling of NLRP3-biomarker signatures with selected reaction monitoring-mass
73 spectrometry (SRM-MS). Finally, ATP Sepharose was used in combination with a fluorescence-
74 linked enzyme chemoproteomic strategy (FLECS) screen to identify potential competitive
75 inhibitors of NLRP3. The identification of a novel benzo[*d*]imidazol-2-one inhibitor that
76 specifically targets the ATP-binding and hydrolysis properties of the NLRP3 protein implies that
77 ATP Sepharose and FLECS could be applied other NLRPs as well.
78
79
80
81
82
83
84
85
86
87
88
89
90
91
92
93
94
95
96
97
98
99
100
101
102
103
104
105
106
107
108
109
110
111
112

113
114
115 **1. The NLRP Inflammasome.** The inflammasome is a protein complex and caspase-activating
116 platform that drives inflammation and plays a crucial role in the innate immune response [1-4].
117
118 Following stimulation by pathogen or danger/damage associated molecular patterns (PAMPs or
119 DAMPs), inflammasome assembly induces the recruitment and autocatalytic cleavage of pro-
120 caspases-1, 8 and 11, which are cysteine proteases and the key effectors of the inflammasome [5-
121 7]. Activated caspases in turn regulate key processes involved in inflammation and host defense
122 that includes cytokine maturation, metabolism, reactive oxygen species (ROS) generation,
123 apoptosis and pyroptosis. For example, pro-IL-1 β , an endogenous pyrogen that induces fever as
124 well as other immune responses, is cleaved by caspase-1 into mature IL-1 β and is released into the
125 extracellular environment to fulfill its physiological functions [8].

136
137 Each inflammasome has scaffold proteins that determine inflammasome specificity and
138 mediate its assembly. The nucleotide-binding oligomerization domain, leucine rich repeat and
139 pyrin domain containing-3 (NLRP3) protein is the most extensively studied inflammasome
140 scaffold protein. This protein belongs to the 14-member NLRP subfamily of the immune sensor
141 Nod-like receptor (NLR) family [9]. NLRP3 possesses an N-terminal pyrin domain (PYD), a
142 central NAIP, CIITA, HET-E and TP1 (NACHT) domain, and a C-terminal leucine rich repeat
143 (LRR) domain [10]. The PYD of NLRP3 has been demonstrated to interact with pro-caspase-1 via
144 an adaptor protein, apoptosis-related speck-like protein (ASC) [11,12]. The NACHT domain binds
145 to and hydrolyzes ATP and contributes to NLRP3 inflammasome assembly and activation [13].
146 Although limited direct evidence has been provided, the LRR domain is thought to be responsible
147 for detecting a wide spectrum of NLRP3 ligands that include nigericin [14], asbestos [15], silica
148 [16], β -amyloid [17], cholesterol crystals [18], fatty acids [19], urate crystals [20], aluminum oxide
149 [16], along with certain engineered nanomaterials [21] and other implanted metal medical devices
150
151
152
153
154
155
156
157
158
159
160
161
162
163
164
165
166
167
168

169
170
171 [22]. Generally, a two-step model has been proposed for canonical NLRP3 activation [23]. First,
172
173 transcriptional priming of NLRP proteins and cytokine precursor proteins is induced via NF- κ B
174
175 signaling. The second step is driven by the accumulation of cellular danger signals, such as ROS
176
177 [15,23], potassium and/or calcium flux [24-26], and/or lysosomal disruption [16,18]. More
178
179 recently, mitochondria have also been demonstrated to play a critical role in NLRP3
180
181 inflammasome assembly [27-31]. In addition, it has been recently reported that RNA binding
182
183 proteins provide post-transcriptional regulation of NLRP3 [99]. Collectively, NLRP3 activity is
184
185 controlled multiple levels with important control also existing at the post-translational level via
186
187 phosphorylation [32-34] and/or ubiquitination [35-37].
188
189

190 **2. NLRPs possess ATP-binding Properties.** Comparative sequence analyses reveal conservation
191
192 within NACHT that designate NLRPs as members of the Signal Transduction ATPases with
193
194 Numerous Domains (STAND) clade within the larger ATPases-Associated with various cellular
195
196 Activities (AAA+ ATPase) superfamily of proteins [38-40]. The vast majority of STAND
197
198 ATPases are modular proteins, containing multiple domains involved in DNA or protein binding,
199
200 signal transduction and scaffolding. STAND proteins have a conserved core, containing enzymatic
201
202 ATPase activity, as well as key domains involved in sensing of stimuli, and effector domains for
203
204 downstream signaling. A conserved mechanism of activation has been proposed, based on the
205
206 structural-function relationships of four different STAND ATPases [41]. Briefly, the integrated
207
208 data suggest that STAND ATPases function as regulated molecular switches, which undergo
209
210 structural reorganizations corresponding to monomeric, resting ADP-bound forms in the off
211
212 position, and ATP-bound, oligomeric forms in the on position, which can signal downstream via
213
214 protein-protein interactions in the aforementioned effector domains.
215
216
217
218
219
220
221
222
223
224

225
226
227 All the different NLRP proteins possess a NACHT domain that is expected to mediate ATP-
228 binding and hydrolysis [9]. A primary sequence alignment of the NACHT domain of each NLRP
229 reveals multiple conserved regions for ATP-binding (e.g., Walker A and Walker B motifs, GxP,
230 motif as well as a Winged-helix domain) [42-44]. Yet, only NLRP3 [13], NLRP7 [45] and
231 NLRP12 [46] have been empirically defined to possess ATP-binding potential and intrinsic
232 ATPase activity. Mutations in the ATP-binding regions (e.g., the Walker A motif) within these
233 specific NLRP proteins abolished their ATP-binding and ATPase activities and thereby resulted
234 in impaired IL-1 β maturation [13,46]. The biochemical assessments employed to date have been
235 quite rudimentary in nature, and a comprehensive kinetic characterization of the enzymatic nature
236 of any NLRP protein has yet to be completed (i.e., K_M for ATP binding, V_{max} for ATP hydrolysis,
237 and turnover number k_{cat}). While it was evident that NLRP1 inflammasome activation was
238 nucleotide dependent [47], the capacity of NLRP1 to hydrolyze ATP is not yet resolved. Although
239 the seminal paper linked the contribution of nucleotide-binding to the functional role of
240 NLRP1[47], a soluble fragment of the protein containing the NACHT domain and the LRR
241 exhibited negligible ability to hydrolyze triphosphate nucleotides [48]. As a whole, the basic
242 enzymology of the NLRPs remains under-characterized, and further description of the role played
243 by the NACHT in driving inflammasome activation and the ensuing inflammatory signaling
244 pathways will be critical for a comprehensive understanding of this family and their role in human
245 disease.

246
247
248
249
250
251
252
253
254
255
256
257
258
259
260
261
262
263
264
265
266
267
268
269
270 **3. Application of Immobilized ATP Supports to the Study of NLRPs.** Many different protein
271 families possess biochemical properties in terms of amino acid sequence and three-dimensional
272 structural folds that enable ATP-binding. Two major groups of enzymes are associated with
273
274
275
276
277
278
279
280

281
282
283 binding of ATP: the AAA+ ATPases and the universal stress protein (USPs) which bind and
284
285 hydrolyze ATP, and the kinases which bind and mediate the transfer of the γ -terminal phosphoryl
286
287 of ATP to another molecule (i.e., to a small molecule by metabolic kinases such as 6-
288
289 phosphofructokinase or to another protein substrate by protein kinases). Historically, biochemical
290
291 studies of these proteins were advanced with the application of immobilized ATP solid support
292
293 resins. These chromatography media are prevalent in the literature for ATP-binding studies and
294
295 for affinity purification of ATP-binding proteins [49-55]. Indeed, the ATP-binding properties of
296
297 NLRP3 were demonstrated using an N-linked ATP Sepharose resin [56]. The protein binding
298
299 efficiency is particularly sensitive to the type of chemistry employed in the ATP linkage. Both the
300
301 physicochemical properties and length of the linker, as well as its position on the ATP molecule
302
303 can interfere with binding, thereby reducing capture efficiency. A variety of different resins can
304
305 be synthesized (Figure 1), and these are typically generated by coupling ATP to the solid support
306
307 matrices via the available reactive groups present on the ribose sugar (R-linked), the adenine base
308
309 (N-linked) or the γ -phosphate (P-linked). Different types and lengths of linker arms (e.g.,
310
311 aminophenyl and alkyl groups spanning up to 10 carbon atom spacers) as well as solid support
312
313 matrices (i.e., Sepharose, agarose and magnetic beads) can be employed to optimize the most
314
315 effective protein binding response.
316
317
318
319
320
321

322 INSERT FIGURE 1 HERE
323
324
325

326 **3.1. Impact of Orientation and Crosslinking on NLRP3 Capture with Immobilized ATP.**

327
328 Structural examinations of the NLRP-related APAF1 and NLRC4 folds have established that both
329
330 proteins adopt closed conformations with the nucleotide buried deeply within the active site [42,
331
332
333
334
335
336

337
338
339 57]. In the nucleotide binding site of APAF1, the N1 and N6 atoms of the adenine ring are
340 coordinated by the main-chain amide and carbonyl groups of Val127 [42]. Likewise, hydrogen
341 bonds between ADP and the NACHT domain of NLRC4 originate from coordination of the N1
342 and N6 atoms in the adenine base [57]. Thus, the hydrogen bond arrangements within the NACHT
343 appear to be adenine specific, and therefore provide a specificity filter to disrupt efficient binding
344 of other nucleotides (e.g., GTP) within the site. Indeed, only adenosine nucleotides were able to
345 competitively elute NLRP3 from N-linked ATP Sepharose [13]. Moreover, studies utilizing a
346 fluorescence polarization assay with NLRP1 revealed that ATP-binding was still permitted with
347 fluorophore addition to the purine; whereas, nucleotide-binding following conjugation of
348 fluorophore to the sugar or γ -phosphate moieties of ATP was not tolerated [47]. Ultimately, the
349 structural topology of nucleotide bound within the NACHT of the APAF1 and NLRC4 suggest
350 that the chemical nature of the ATP Sepharose capture resin, with modification of linker types,
351 lengths and properties, could significantly impact upon binding affinity and recovery of NLRPs.
352
353
354
355
356
357
358
359
360
361
362
363
364
365
366
367
368

369 INSERT FIGURE 2 HERE
370
371
372

373
374 The effect of the molecular linkage of ATP to the Sepharose bead on NLRP3 protein capture
375 efficiency was examined herein by comparing the binding capacity of five ATP Sepharose
376 matrices under conditions of ligand saturation (Figure 2). The P-linked ATP Sepharose was
377 generated by coupling to Sepharose via the γ -phosphate group [69]. The N-linked Sepharoses were
378 generated by coupled through the N6- and N8- amino groups of the purine ring of the nucleotide,
379 respectively. The R-linked ATP Sepharose was a mixed-bed of ATP coupled to the hydroxyls at
380 either the C2 or C3 position of the ribose ring. Importantly we identify the NLRP3-ligand binding
381
382
383
384
385
386
387
388
389
390
391
392

393
394
395 efficiency to be particularly sensitive to the ATP linkage. The capture efficiency observed with the
396
397 P-linked ATP Sepharose was the highest, at $96.1 \pm 2.4\%$, varying with the binding ratio of cell
398
399 lysate to Sepharose. The binding efficiency of N6-linked ATP Sepharose was low, at $23.9 \pm 9.1\%$,
400
401 while coupling at the N8 position resulted in an increase in capture efficiency to $47.1 \pm 5.9\%$. The
402
403 R-linked ATP Sepharose was the least effective for NLRP3 capture, at $18.4 \pm 7.4\%$. Each binding
404
405 experiment was performed by incubating whole cell lysates (HEK293T, stably-expressing
406
407 NLRP3-GFP) with ATP Sepharose at a volumetric ratio of 1:2 (lysate:matrix). The capture
408
409 efficiency was not impacted with ratiometric increase to 1:4 (lysate:matrix), indicating that ATP
410
411 ligand concentrations were always supersaturating. Immunoblotting analysis of NLRP3 captured
412
413 from transiently-transfected HEK293T cells confirmed that the GFP tag did not interfere with the
414
415 ability to capture NLRP3 on P-linked ATP-Sepharose (Figure 3A), and endogenous NLRP3
416
417 protein could also be captured from THP-1 cells with the affinity resin (Figure 3B). Lastly, a
418
419 cleavable P-linked ATP Sepharose, whereby the ATP molecule (and bound protein) can be cleaved
420
421 from Sepharose through the reduction of a diazo bond with sodium dithionite could also prove
422
423 beneficial for protein capture applications (Figure 2). In this case, NLRP3 binding efficiency to
424
425 the cleavable diazo-P-linked ATP Sepharose was slightly reduced as compared to the non-
426
427 cleavable P-link, at $82.3 \pm 1.5\%$, suggesting that the chemical identify of the linker used to secure
428
429 the ATP molecule to the solid support also impacts on binding efficiency.
430
431
432
433
434
435

436 INSERT FIGURE 3 HERE
437
438
439

440 The ligand density of ATP Sepharose was previously suggested to play a role in the capture
441
442 efficiency of larger proteins [58]. This was postulated to result from steric hindrance generated by
443
444
445
446
447
448

449
450
451 higher molecular weight proteins on the beads, occluding the access and binding of proteins to
452 proximate ATP molecules. As the NLRP proteins are quite large, ranging from 75 kDa to 170 kDa,
453 we initially hypothesized that lowering the immobilized ligand density might improve the capture
454 efficiency. However, enhanced NLRP3 capture was observed with increased concentration of
455 immobilized ATP (Figure 4A). At the lowest ligand density (0.1 $\mu\text{mol ATP/mL Sepharose}$), less
456 than 20% of the input NLRP3 was captured; while $\sim 80\%$ of the NLRP3 input was retained on the
457 column with the highest ligand density (0.25 $\mu\text{mol ATP/mL Sepharose}$). We also observed an
458 increase in the competitive elution potential with free [ATP] as the immobilized ligand density on
459 the Sepharose beads was decreased (Figure 4B & 4C). Although significantly less NLRP3 could
460 be recovered on the resin, a greater proportion of the captured protein could be competitively eluted
461 at free [ATP] less than 50 mM. One potential explanation could be an increased capacity of the
462 free ATP molecule to access the NLRP3 binding pocket at lower immobilization densities.
463 Another could be that reducing the immobilized [ATP] on the beads could attenuate any localized
464 rebinding of NLRP3 protein back to the beads after elution. Surprisingly, the maximal NLRP3
465 recovery with competitive elution using high free [ATP] (i.e., 200-300 mM) was only $\sim 40\%$
466 (Figure 4C & 4D). We attribute this phenomenon to localized rebinding effects whereby the
467 displaced NLRP3 is able to re-engage the immobilized ATP ligand. Alternatively, NLRP3 protein
468 in the ATP-bound state may adopt a conformation that requires additional effectors to permit its
469 release from the immobilized ligand. For example, additional protein interactions (e.g., ASC
470 binding upon inflammasome assembly) may be required to facilitate nucleotide exchange from the
471 NACHT domain in a mechanism analogous to the binary switching of small G-protein cycling
472 between GDP-bound, inactive and GTP-bound, active states. Finally, we are uncertain as to the
473 reason for loss of NLRP3 recovery from low ligand density P-linked ATP Sepharose resins (i.e.,
474
475
476
477
478
479
480
481
482
483
484
485
486
487
488
489
490
491
492
493
494
495
496
497
498
499
500
501
502
503
504

505
506
507 < 0.15 $\mu\text{mol ATP/mL Sepharose}$) with high free [ATP] (Figure 4C & 4D). We speculate that
508 perhaps protein was lost as aggregates on the column due to NLRP3 oligomerization under these
509 conditions.
510
511
512
513

514
515
516 INSERT FIGURE 4 HERE
517

518
519
520 **3.2. Application of Immobilized ATP for Proteomic Studies of NLRPs.** The integration of
521 NLRPs into prognostic and diagnostic assays has been hampered by the number and complexity
522 of inflammasomes, the scarcity of selective antibodies, and the similarity of the family members.
523
524 Mass spectrometry (MS) – based targeted proteomics with selected reaction monitoring (SRM) is
525 a powerful method for quantification of many dozens of proteins in a single analytical run [59-61].
526
527 SRM-MS relies on the detection of a prototypic peptide derived from the protein ‘biomarker’. This
528 peptide can be selectively filtered and quantified against an internal reference standard (e.g. a,
529 stable isotope-labeled synthetic peptide, SIS peptide) to yield absolute protein concentration.
530
531 SRM-MS has an advantage over antibody-based quantitative methods in that it is only dependent
532 on knowledge of tryptic peptide masses that can be easily derived from the protein sequence.
533
534
535
536
537
538
539
540
541
542

543 INSERT TABLE 1 HERE
544
545
546
547

548 The NLRP family has not been previously examined with SRM-MS, so we initially
549 completed a comprehensive *in silico* assessment of annotated proteomic databases to define
550 candidate peptides for experimental validation [62,63]. The proteotypic SRM-MS peptides for the
551 different NLRP members take into account annotated single nucleotide polymorphisms (SNPs)
552
553
554
555
556
557
558
559
560

561
562
563 and splice variants that ensure independence from genetic variability of samples [64]. Potential
564 post-translational modification sites were also considered in refining the peptide choices. As a pilot
565 study, an SRM-MS survey scan for NLRP3 was constructed using Skyline and transitions were
566 empirically confirmed [65]. An empirical validation of SRM-MS peptide choices was completed
567 using heterologous cellular expression of NLRP3 in HEK293 cells. SRM-MS analyses of HEK293
568 cell extracts recorded 27 peptides with mass ranges of 6 to 21 amino acids that covered ~25% of
569 the NLRP3 sequence (Table 1). For bioinformatic verification, peptides were checked using the
570 SRM collider program [66]. The observed fragments were also compared to the NIST and GPMDB
571 databases to ensure uniqueness [67]. Based on its high signal-to-noise ratio, the peptide
572 GDILLSSLIR was selected as a reasonable proteotypic candidate peptide for NLRP3. This peptide
573 is adjudged to satisfy the criteria for successful SRM-MS application, including signal-to-noise
574 character, peptide storage stabilities, reproducible chromatography capture and elution, MS/MS
575 confirmation of peptide identity, and transition selections. For quantitative applications, an
576 isotope-labelled internal standard (SIS peptide) can be used as an internal calibrant for the
577 GDILLSSLIR peptide to generate an absolute measure of NLRP3 abundance. For quantitation,
578 specific signals (peak areas) derived from the endogenous unlabeled species can be compared to
579 those from the SIS peptides to calculate concentrations.
580
581
582
583
584
585
586
587
588
589
590
591
592
593
594
595
596
597
598

600
601 INSERT FIGURE 5 HERE
602
603
604
605

606 Crude protein extracts (e.g., cell or tissue extracts as well as body fluids such as urine and
607 blood) can be used for SRM-MS. However, in practice many proteins exist below the level of
608 SRM-MS detection unless enrichment strategies are employed to boost signal for effective
609
610
611
612
613
614
615
616

617
618
619 quantitation. It is disappointing that NLRP proteins have not emerged as useful targets for SRM-
620 MS biomarker assays despite great interest in the field. Indeed, we could not reproducibly detect
621 the proteotypic NLRP3 peptide GDILLSSLIR (as well as other tryptic peptides) by SRM-MS in
622 cell extracts of PMA-differentiated THP-1 cells following nigericin stimulation (Figure 5), even
623 though the presence of NLRP3 protein is routinely confirmed under these conditions by western
624 immunoblotting. Although the NLRP inflammasomes are generally under-represented in
625 biomarker surveys due to factors that preclude their facile detection (e.g., low-expression levels
626 and peculiar biophysical characteristics), NLRP3 protein can be identified using untargeted MS
627 approaches [68]. So, we applied P-linked ATP Sepharose as a tool for the examination of NLRP3
628 protein in crude cellular lysates. In this regard, P-linked ATP Sepharose provided effective capture
629 and enrichment of NLRP3 for SRM-MS reporting (Figure 5). NLRP3 was readily identified from
630 four unique peptides with three to five transitions for each. Peak areas of the highest transition (as
631 determined by Skyline) were used as a readout of relative expression, and peptide intensities below
632 the detection limit were excluded. Signal detection was improved (~20-fold) by sample processing
633 with immobilized ATP prior to the SRM-MS analysis. This improvement was achieved through
634 concentration of NLRP3 protein in the whole cell extract as well as a reduction in the background
635 signal generated during the SRM-MS run. The results also suggest that distinct relative intensities
636 for different peptides could be elicited, most likely due to differences in access to tryptic cleavage
637 sites for ATP-bound NLRP3. Again, the results support the potential use of the GDILLSSLIR
638 peptide as a reasonable proteotypic candidate for quantitation of NLRP3 following capture with
639 immobilized ATP supports.
640
641
642
643
644
645
646
647
648
649
650
651
652
653
654
655
656
657
658
659
660
661
662
663
664
665
666
667
668
669
670
671
672

673
674
675 **3.3. Application of immobilized ATP with FLECS in NLRP drug discovery.** The P-linked ATP
676
677 Sepharose matrix has been successfully employed in chemoproteomic applications for the rapid
678
679 screening of drug candidates (e.g., Fluorescence-linked Enzyme Chemoproteomic Strategy
680
681 (FLECS)) [69-73]. At the core of the FLECS method is the capture of a fluorescently-tagged target
682
683 protein with immobilized ATP in the presence of the entire cellular purinome. Selective drug
684
685 candidates can then be identified by their ability to provide competitive elution of the
686
687 fluorescently-tagged target. While earlier chemoproteomic technology was originally applied to
688
689 profile protein kinases [56,74]; recent studies reveal that metabolic enzymes and other non-kinase
690
691 purine-utilizing proteins can also be effectively screened with proteome mining using this ATP
692
693 Sepharose platform [70,71,73]. Herein, we have applied FLECS with P-linked ATP Sepharose as
694
695 a means to screen for NLRP3-interacting small molecules by exploiting the nucleotide-binding
696
697 properties of the NACHT domain.
698
699
700
701

702
703 INSERT FIGURE 6 HERE
704
705
706

707 As a first step, we examined the capture and elution of various GFP-tagged NLRP family
708
709 members from P-linked ATP Sepharose using FLECS. Various NLRP-GFP fusion proteins were
710
711 expressed in HEK293T cells, and crude lysates were combined with P-linked ATP Sepharose
712
713 without further purification. All of the NLRP proteins profiled could be captured and competitively
714
715 eluted with ATP (Figure 6A & 6B, respectively). No change in fluorescence intensity was
716
717 observed for ATP elutions when cell lysates containing expressed GFP were used as controls (data
718
719 not shown). A significant portion of NLRP-GFP protein remained bound to the affinity resin even
720
721 with high super-saturating ATP concentrations. This is primarily a result of a rebinding effect
722
723
724
725
726
727
728

729
730
731 wherein competitively inhibited proteins immediately experience a high local concentration of
732 immobilized ATP and rebind to the resin instead of eluting. In some cases, the capture of
733 fluorescence signal from cell lysates with ATP Sepharose during FLECS did not correlate with
734 changes in NLRP protein capture as judged by immunoblotting (Figure 6C). Differences with
735 intrinsic fluorescence due to environmental distinctions between the load and unbound fractions
736 may account for this observation. So, the recovery of NLRP-GFPs from the ATP Sepharose during
737 FLECS was also confirmed by immunoblotting the ATP elution fractions. Ultimately, sufficient
738 amounts of NLRP-GFP proteins (except NLRP2-GFP) were captured and competitively eluted
739 with ATP to enable application of the FLECS method to the NLRP family. Interestingly, the
740 efficiency of NLRP2 elution during FLECS was low and negligible amounts of protein were
741 detected by western blotting. Given that the motifs important for ATP-binding are conserved in
742 the NACHT domain of NLRP2 [43,44], it is unclear what accounted for this distinction in binding
743 character.

744
745 The FLECS chemoproteomic strategy was used to identify molecules that act in an ATP-
746 competitive manner towards fluorescence-linked NLRP3 (Figure 7A). First, NLRP3-GFP protein
747 in HEK293T crude lysates was directly loaded onto P-linked ATP-Sepharose beads without further
748 purification. Charged beads were washed and then distributed into each well of a 96-well filter
749 plate in order to screen a library of 3,379 compounds as a test case. A description of the selection
750 criteria for the constituents of the compound library was provided previously [69]. In brief, the
751 compound library was assembled with attention to commercial availability, structural diversity,
752 similarity to known inhibitors of purine-binding proteins, as well as any identifiable reactive
753 liabilities. After elution, the fluorescence of each sample was determined, and a threshold was set
754 to differentiate “positive hits” from inactive drug candidates. The positive hits were further

785 confirmed by immunoblotting for NLRP3-GFP protein. Approximately 120 positive hits (3.5% hit
786 rate) were observed with FLECS for NLRP3. Those compounds providing a 5-fold increase in
787 fluorescence signal over background during FLECS were classified as a positive hit. This value
788 was chosen since it was reflective of the signal development at the EC₅₀ for ATP elutions. The
789 positive FLECS hits were further confirmed with secondary screening by immunoblotting. This
790 analysis revealed nine lead compounds with positive immunoreactivity to NLRP3-GFP protein in
791 the elutions. Some compounds result in false positive reports since they possess intrinsic
792 fluorescence properties; these molecules were recorded as positive hits during the FLECS screen
793 but were unable to provide positive immunoreactivity on confirmatory analyses. The suitability of
794 FLECS as a method to screen a library of compounds for their ability to displace ATP-bound
795 NLRP3 was confirmed with a calculated Z' factor of 0.61 [75]. Furthermore, the robustness of
796 FLECS was reflected by its utility in assessing proteins that are not amenable to traditional high-
797 throughput screening (HTS). In the case of NLRP drug discovery, FLECS provided a means to
798 circumvent issues with recombinant NLRP protein expression and the lack of practical HTS assay
799 for enzymatic activity profiling.
800
801
802
803
804
805
806
807
808
809
810
811
812
813
814
815
816
817
818
819

820
821 INSERT FIGURE 7 HERE
822
823
824

825 NLRP3 inflammasome activation can trigger multiple cellular effects in myeloid cells such
826 as macrophages and dendritic cells, a major one being IL-1 β secretion [5,13,76,77]. Next, we
827 addressed whether the compounds could affect IL-1 β release triggered by NLRP3 inflammasome
828 activation. Differentiated THP-1 cells, a human monocytic cell line, were either left untreated or
829 exposed to extracellular ATP in the absence or presence of the compounds. HS203873, a
830
831
832
833
834
835
836
837
838
839
840

841
842
843 benzo[d]imidazol-2-one compound, was the most effective attenuator of ATP-induced IL-1 β
844 secretion, to ~35% of the vehicle control (Figure 7B). In addition, compound HS206461 showed
845 some inhibitory potential on ATP-induced IL-1 β secretion. Moreover, administration of
846 compound HS206364 routinely enhanced IL-1 β secretion from THP-1 cells. Elevated levels of IL-
847
848 1 β were detected when cells were treated alone with HS206364 or in combination with
849 extracellular ATP as an activator of NLRP3 inflammasomes. Likewise, treatment of THP-1 cells
850 with HS206537 also resulted in augmented IL-1 β secretion. The significance of this stimulatory
851 effect is not clear, and we did not pursue additional investigations. Six of the compounds had no
852 obvious effect on NLRP3 inflammasome activity in the cell assay, suggesting they have poor
853 bioavailability.
854
855
856
857
858
859
860
861
862
863
864

865 Based on these results, we pursued further examination of HS203873. Differentiated THP-1
866 cells were primed with LPS and treated with ATP and increasing [HS203873], then cell
867 supernatants were collected to probe maturation of pro-IL-1 β and pro-caspase-1. Increasing
868 concentrations of HS203873 caused greater reductions in IL-1 β secretion triggered by extracellular
869 ATP exposure (Figure 7C). The NLRP3 inflammasome also regulates pro-caspase-1 processing,
870 and influences the profile of multiple processed caspase-1 fragments (e.g., p10, p20 and p11-
871 CARD) that are secreted into the extracellular environment [100]. HS203873 consistently
872 prevented ATP-triggered NLRP3 activation and pro-caspase-1 maturation (Figure 7D). Taken
873 together, these studies suggest that HS203873 could antagonize NLRP3 inflammasome activation
874 following exposure to a DAMP (i.e., extracellular ATP).
875
876
877
878
879
880
881
882
883
884
885
886

887 The results of THP-1 cell-based experiments collectively suggest that HS203873 could
888 inhibit pro-caspase-1 cleavage and IL-1 β secretion via inhibition of the NLRP3 inflammasome.
889 To directly examine the ability of HS203873 to attenuate NLRP3 inflammasome assembly, we
890
891
892
893
894
895
896

897
898
899 reconstituted the NLRP3 inflammasome in HEK293T cells, which are deficient in NLRP
900 inflammasome components, by co-expressing NLRP3-GFP and FLAG-NLRP3 tagged variants.
901
902 By monitoring the co-incident pull-down of NLRP3-GFP during immunoprecipitation with anti-
903 FLAG antibody, we demonstrate the spontaneous assembly of a multimeric NLRP3 complex
904 (Figure 8A). The treatment of HEK293T cells with HS203873 provided concentration dependent
905 attenuation of NLRP3 oligomerization *in situ* (Figure 8B). HS203873 occupation of the NACHT
906 domain was expected to inhibit the ATP hydrolysis properties of NLRP3, and we performed *in*
907 *vitro* ATPase assays using fluorometric detection of ADP. Immunoprecipitated NLRP3-GFP could
908 elicit ATP hydrolysis and ADP production (Figure 8C). Importantly, incubation with HS203873
909 (100 μ M) could suppress the ATP hydrolysis potential of NLRP3. The concentration-dependent
910 elution of NLRP3-GFP from P-linked ATP Sepharose (Figure 8D) with HS203873 was also
911 assessed. In this case, increasing amounts of GFP-tagged NLRP3 were eluted as concentrations of
912 HS203873 were elevated. As an alternative to the elution approach, we observed the ability of
913 HS203873 to impede NLRP3-GFP binding with immobilized ATP (Figure 8E). Pre-incubation of
914 the cell lysate with increasing concentrations of HS203873 resulted in attenuated capture of
915 NLRP3 protein with immobilized ATP (i.e., more NLRP3 protein remained in the unbound
916 fraction). Although the results support the direct action of HS203873 on NLRP3-dependent ATP
917 hydrolysis and inflammasome assembly, the possibility remains that other components of the
918 inflammasome pathway are also affected. In this regard, additional experiments will need to
919 address whether the compound has any impact on NF- κ B and the expression of NLRP3 during
920 priming. Moreover, additional structure-activity relationship (SAR) studies will be necessary to
921 increase the selectivity and potency of the HS203873 pharmacophore. Given that the majority of
922 the structural information for NLRP3 has been derived from *in silico* models, more biochemical
923
924
925
926
927
928
929
930
931
932
933
934
935
936
937
938
939
940
941
942
943
944
945
946
947
948
949
950
951
952

953
954
955 evidence will be helpful to complete our understanding of how the NACHT domain of NLRP3
956
957 interacts with ATP-competitive inhibitors.
958
959
960

961
962 INSERT FIGURE 8 HERE
963
964
965

966 Over the past several years, many small molecules have been reported to block NLRP3
967
968 inflammasome activation (Table 2), yet the mechanism for antagonism by most of these
969
970 compounds generally appears to be indirect in nature. The cytokine release inhibitory drugs
971
972 (CRID, diarylsulfonylureas) can prevent IL-1 β secretion [78]. The ability of CRID3 to attenuate
973
974 ATP-induced IL-1 β post-translational processing is suggested to occur through its targeting of
975
976 glutathione S-transferase omega 1-1 [79]. Later studies demonstrated that CRID3 could attenuate
977
978 ASC-dependent inflammasome assembly and caspase-1 processing by NLRP3 and AIM2, but not
979
980 by NLRC4 [80]. The inhibitory action of CRID3 is thought to involve glutathione S-transferase
981
982 omega regulation of the interaction of ASC with NLRP3 and maintenance of the inflammasome
983
984 complex. Most recently, a diarylsulfonylurea termed MCC950 was reported to possess high
985
986 potency and specificity for NLRP3-dependent IL-1 β production [81]. The precise molecular
987
988 mechanism of action for MCC950 on the NLRP3 inflammasome has not been ascertained;
989
990 however, the molecule may interact directly with NLRP3 or block NLRP3 homo- and/or hetero-
991
992 oligomerization. Given the heterocyclic nature of MCC950, it is possible that the molecule may
993
994 occupy the ATP-binding site of the NACHT domain and attenuate the ATPase activity of NLRP3.
995
996 Luteoloside, a flavonoid, can also attenuate NLRP3-associated caspase-1 processing and IL-1 β
997
998 secretion, and its effect is likely associated with a suppression of intracellular ROS [82].
999
1000 Andrographolide was demonstrated to inhibit NLRP3 activation in macrophages [83]; however,
1001
1002
1003
1004
1005
1006
1007
1008

1009
1010
1011 its mechanism of action was determined to be via mitophagy and reversal of mitochondrial
1012 membrane potential disruption. In addition, bromoxone inhibits NLRP3 activation in a
1013 transcription-independent manner [84]. Glyburide, an ATP-sensitive potassium channel inhibitor,
1014 can suppress the NLRP3-dependent maturation of pro-caspase-1 and pro-IL-1 β [85]. In addition,
1015 a small molecule intermediate in the synthesis of glyburide (i.e., the so called 16673-34-0
1016 compound) was also able to inhibit the formation of the NLRP3 inflammasome [86]. Rather than
1017 acting directly on the NLRP3 protein, glyburide and its synthetic precursor likely targets an
1018 upstream effector of NLRP3 inflammasome activation (i.e., K⁺ efflux). The benzo[*d*]imidazole
1019 Fc11a-2 was shown to attenuate the release of caspase-1 from ASC/NLRP3 complexes in response
1020 to ATP-stimulation of LPS-primed THP-1 cells [87]. Bay 11-7082, a known NF- κ B inhibitor, was
1021 also shown to block NLRP3 inflammasome activation [88]. One potential mechanism for Bay 11-
1022 7082 may be that it inhibits linear ubiquitin complex formation which was recently demonstrated
1023 to be essential for NLRP3 activation [89,90]. Moreover, 3,4-methylenedioxy- β -nitrostyrene was
1024 proposed to inhibit NLRP3 by blocking assembly of the inflammasome [91]. Intriguingly, both
1025 3,4-methylenedioxy- β -nitrostyrene and Bay 11-7082 were shown to inhibit NLRP3 ATPase
1026 activity [88,91]. Although the exact role of ATP hydrolysis in inflammasome assembly and
1027 activation has not yet been empirically defined, it is possible that these two compounds inhibit the
1028 ATPase activity of NLRP3 by occupying the ATP-binding pocket within the NACHT domain.
1029 This would be in line with our identification of novel ATP-competitive small molecules that can
1030 be applied for the selective inhibition of the NLRP3 inflammasome.
1031
1032
1033
1034
1035
1036
1037
1038
1039
1040
1041
1042
1043
1044
1045
1046
1047
1048
1049
1050
1051
1052
1053
1054
1055

1056 INSERT TABLE 2 HERE
1057
1058
1059
1060
1061
1062
1063
1064

1065
1066
1067
1068
1069
1070
1071
1072
1073
1074
1075
1076
1077
1078
1079
1080
1081
1082
1083
1084
1085
1086
1087
1088
1089
1090
1091
1092
1093
1094
1095
1096
1097
1098
1099
1100
1101
1102
1103
1104
1105
1106
1107
1108
1109
1110
1111
1112
1113
1114
1115
1116
1117
1118
1119
1120

Our identification of a novel pharmacophore that specifically competes against ATP-binding of the NLRP3 protein implies that the ATP-binding pockets of the other NLRPs could be attractive therapeutic targets as well. A few concerted efforts have been made to identify compounds that specifically target the NLRP3 protein. For example, a library of electrophilic ‘warhead’ molecules possessing α,β -unsaturated nitrile- or carbonyl-derived functionalities were produced by Cocco and colleagues [92]. The prototypical compound (*Compound 9*, with α,β -unsaturated lactone substructure) could directly inhibit caspase-1 and NLRP3 ATPase activities presumably by the irreversible alkylation of regulatory cysteine residues. Additional tuning of the electrophilic warhead reactivity has yielded compounds that irreversibly target NLRP3 with reduced cytotoxicity (e.g., acrylamide derivatives [93] and INF39 [94]). Moreover, Jiang and colleagues recently identified a compound (i.e., CY-09) that binds directly to the NACHT domain and inhibits ATPase activity with associated attenuation of NLRP3 inflammasome assembly [95]. All of the NLRP proteins possess a NACHT domain that presumably binds to ATP, and the importance of ATP binding/hydrolysis in the function of several NLRPs has been demonstrated. The primary sequence alignment of the NACHT domain of each NLRP not only reveals multiple conserved regions for ATP-binding (e.g., Walker A, Walker B and GxP motifs as well as the winged-helix domain) but also identify several distinct amino acids in the ATP-binding pocket. This sequence heterogeneity is predicted to offer a selectivity filter and support the opportunity for development of specific ATP-competitive compounds for each NLRP protein. As ATP elution curves for other NLRP proteins have been generated (Figure 6B & 6C), this drug discovery platform could be applied to identify small molecules that target select members of the NLRP family.

4. Materials and Methods

1121
1122
1123 *Reagents-* ATP, phorbol 12-myristate 13-acetate (PMA), glyburide, puromycin and N6-linked
1124 ATP-Sepharose were purchased from Sigma Chemical Co (St. Louis, MO). All other chemicals
1125 were of reagent grade and were obtained from VWR (Edmonton, AB) or Sigma Chemical Co. P-
1126 linked γ -aminodecyl ATP Sepharose was synthesized at Duke University using published
1127 protocols [50,69]. Other immobilized ATP resins (R-linked and N8-linked ATP Sepharose resins)
1128 were obtained from Jena Bioscience GmbH (Germany). Bay 11-7082 was from Enzo Life Sciences
1129 (Farmingdale, NW). Mouse anti-human NLRP3 (Cryo-2, Adipogen, San Diego, CA), mouse anti-
1130 human IL-1 β (Cell Signaling, Danvers, MA), rabbit anti-human caspase-1 (sc-622, Santa Cruz,
1131 Dallas, TX), mouse anti-FLAG M2 (F1802, Sigma Chemical Co.), and rabbit anti-GFP (sc-8334,
1132 Santa Cruz) were used for immunoblotting. Sequencing-grade modified trypsin (#V5111) was
1133 purchased from Promega Corp. (Madison, WI). The lead candidate compounds were purchased
1134 from Enamine (HS206461, HS206349, HS203903, HS206327, HS206537, HS206364 and
1135 HS203873), LifeChemicals (HS208040) or Peakdale Molecular (HS208456). CNBr-activated
1136 Sepharose 4B media, anti-rabbit IgG coupled to horseradish peroxidase, and the Enhanced
1137 Chemiluminescence Kit were obtained from GE Healthcare.

1153
1154
1155
1156
1157 *Synthesis of cleavable P-linked diazo-ATP Sepharose-* (E)-4-((5-(2-((tert-
1158 butoxycarbonyl)amino)ethyl)-2-hydroxyphenyl)diazanyl)benzoic acid (30 mg, 78 μ mol; [98]) was
1159 dissolved in methylene chloride (3 mL) and treated with TFA (1.2 mL). After 1 h, the mixture
1160 was concentrated to a glass, then concentrated from ethanol (6 mL) twice. The amine product was
1161 dissolved in DMF (900 μ L) for addition to the resin. In a 50 mL column, CNBr-activated
1162 Sepharose 4B (3 g) was swelled in 1 mM HCl (30 mL) and then washed with 1 mM HCl (600
1163 mL). The resin was washed with coupling buffer (30 mL) and then slurried with coupling buffer

1177
1178
1179 (15 mL). The mixture was then treated with the amine described above (450 μ L of the 900 total).
1180
1181 The mixture was tumbled at room temperature overnight. The resin was then drained (little to no
1182 color eluted) and washed with coupling buffer (5 x 15 mL; 0.1 M NaHCO₃, 0.5 M NaCl, pH 8.3),
1183
1184 diluted with more coupling buffer (~15 mL) and treated with capping solution (300 μ L; 1 M
1185 ethanolamine) and rotated for 1.5 h. The solution was drained and washed with 4 rounds of 21 ml
1186 high buffer (0.1 M AcOH/NaAcOH, 0.5 M NaCl, pH 8) and low buffer (0.1 M AcOH/NaAcOH,
1187 0.5 M NaCl, pH 4). The resin was drained then washed with coupling buffer (3 x 15 mL), diluted
1188 with more coupling buffer (~15 mL) and treated with EDC (298 mg, 1.55 mmol), HOBT (210 mg,
1189 1.55 mmol) and 1,19-diamino-4,7,10,13,16-pentaoxonadecane (240 mg, 0.78 mmol) and rotated
1190 at room temperature for 3 d. The solution was drained and washed with 4 rounds of high buffer/low
1191 buffer (21 mL ea.). The resin was drained then washed with coupling buffer (2 x 15 mL), diluted
1192 with more coupling buffer (~15 mL) and treated with EDC (298 mg, 1.55 mmol), N-
1193 methylimidazole (319 mg, 3.9 mmol) and ATP (885 mg, 1.55 mmol) and rotated at room
1194 temperature overnight. The solution was drained and washed with 4 rounds of high buffer (21 mL
1195 ea.) and then washed with storage buffer (3 x 15 mL) and transferred with storage buffer (20 mL;
1196 0.1M KH₂PO₄, pH 7.4 with 200 mg NaN₃/L) to a vial and stored in the dark at 4 °C until use.
1197
1198
1199
1200
1201
1202
1203
1204
1205
1206
1207
1208
1209
1210
1211
1212
1213
1214

1215
1216 *Preparation of NLRP-GFP Expression Plasmids-* NLRP clones were obtained from various
1217 sources: NLRP1 (NM_033004.3, a gift of Dr. Jeremy Mogridge, University of Toronto); NLRP2
1218 (NM_001174081.1, Origene Cat# RC20201357); NLRP3, (NM_004895.4, Origene Cat#
1219 RG220952); NLRP4 (NM_134444.4, University of Lausanne); NLRP6 (NM_138329.2, Creative
1220 Biogene Cat# CDFG007883); NLRP7 (NM_001127255.1, TransOMIC Technologies Cat#
1221 TCH1003); NLRP8 (NM_176811.2, Origene Cat# RC218775); NLRP9 (NM_176820.3, Origene
1222
1223
1224
1225
1226
1227
1228
1229
1230
1231
1232

1233
1234
1235 Cat# RC213515); NLRP10 (NM_176821.3, Origene Cat# RC211215); NLRP11 (NM_145007.3,
1236
1237 Origene Cat# RC203852); NLRP12 (NM_144687.3, University of Lausanne); and NLRP14
1238
1239 (NM_176822.3, Origene Cat# RC215050). NLRP genes were amplified by PCR, and then
1240
1241 subcloned with restriction digest into the pAcGFP-N1 vector (ClonTech, Cat# 632469). In some
1242
1243 cases, site-directed mutagenesis was performed in order to revert coding-mutations introduced by
1244
1245 PCR in NLRP clones to the wild-type sequence associated with the provided gene accession
1246
1247 number.
1248
1249
1250
1251

1252 *Cell culture-* HEK293T cells (ATCC# CRL-11268) were cultured in Dulbecco's modified Eagle
1253
1254 medium (DMEM) supplemented with 10% (v/v) fetal bovine serum (FBS) and 1% (w/v)
1255
1256 penicillin-streptomycin. Human myelogenous leukemia THP-1 cells (ATCC# TIB-202) were
1257
1258 maintained at 37 °C and 5% CO₂ in RPMI 1640 media supplemented with 10% (v/v) FBS, 1%
1259
1260 (w/v) penicillin-streptomycin, 1% (w/v) sodium pyruvate and 50 μM β-mercaptoethanol. THP-1
1261
1262 cells (10⁵ per well) were seeded and differentiated with 100 nM phorbol-12-myristate-13-acetate
1263
1264 (PMA) in 96-well plate for 16 h prior to all experiments. Differentiated cells were exposed to
1265
1266 lipopolysaccharide (LPS; 1 ng/mL) for 3 h prior to media exchange and treatment with
1267
1268 extracellular ATP (5 mM) in the absence or presence of small molecule inhibitors of the NLRP3
1269
1270 inflammasome.
1271
1272
1273
1274
1275

1276 *IL-1β ELISA and immunoblot analysis of pro-caspase-1 processing-* After treatments, THP-1 cell
1277
1278 supernatants were collected for IL-1β measurement using ELISA (BD Bioscience, Cat# 557966)
1279
1280 according to manufacturer's instructions. Assays were performed in triplicate for each independent
1281
1282 experiment. For the pro-caspase-1 processing assay, supernatants were mixed with SDS-PAGE
1283
1284
1285
1286
1287
1288

1289
1290
1291 loading dye and then subjected to immunoblotting using a polyclonal anti-caspase-1 antibody
1292
1293 (Santa Cruz, Cat# sc622) at 1:500 dilution.
1294

1295
1296
1297
1298 *Cell transfection and generation of stable cell line expressing NLRP3-GFP-* For transient
1299 transfections, the various NLRP-GFP plasmids were transfected into HEK293T cells (~70%
1300 confluent) in a 100-mm petri-dish using 15 μ L PolyJet transfection reagent (SigmaGen
1301 Laboratories). In order to generate a stable cell line that expressed NLRP3-GFP, pCMV6-A-puro
1302 plasmid (10 μ g DNA) encoding NLRP3-GFP was transfected into HEK293T cells in a 100-mm
1303 petri-dish using 30 μ L Lipofectamine 2000 (Invitrogen). Approximately 24 h after transfection,
1304 the DMEM culture media was removed and replaced with DMEM containing 5 μ g/mL puromycin
1305 (Sigma Chemical Co.) to select cells for stable integration of the NLRP3-GFP expressing plasmid.
1306
1307
1308
1309
1310
1311
1312
1313
1314
1315
1316

1317 *Drug candidate screening by FLECS-* The P-linked ATP Sepharose chromatography resin was
1318 prepared as described previously [69]. Crude lysates of HEK293T cells stably expressing
1319 recombinant NLRP3-AcGFP were combined with P-linked ATP Sepharose (1:1 slurry, >50,000
1320 fluorescence counts per 50 μ L of ATP Sepharose slurry) in Lysis Buffer (0.1% (v/v) Triton X-
1321 100, 150 mM NaCl, 60 mM MgCl₂, 25 mM Tris-HCl pH 7.5 containing 1 μ M microcystin-LR and
1322 Complete protease inhibitor cocktail (EDTA-free, Roche) for 1 h at 4 °C. The buffer was removed
1323 by filtration, and the media was washed with 10 column volumes of high salt wash buffer (HSWB;
1324 50 mM Tris-HCl pH 7.5, 1 M NaCl, 60 mM MgCl₂, 1 mM DTT) followed by 10 column volumes
1325 of low salt wash buffer (LSWB; 50 mM Tris-HCl pH 7.5, 150 mM NaCl, 60 mM MgCl₂, 1 mM
1326 DTT). LSBW was then added to the resin, and the resulting 1:1 slurry was distributed into a 96-
1327 well filter plate (50 μ L per well). Positive control: ATP solution (90 μ L, 1-400 mM in LSBW with
1328
1329
1330
1331
1332
1333
1334
1335
1336
1337
1338
1339
1340
1341
1342
1343
1344

1345
1346
1347 10% (v/v) DMSO) was added to control wells. Drug candidate screen: drug candidate (90 μ L in
1348
1349 LSWB with 10% (v/v) DMSO; final concentration of 580 μ M) was added to the remaining wells.
1350
1351
1352 After 10 min of incubation at room temperature, the filtrates were isolated by centrifugation into
1353
1354 black 96-well catch plates (Costar 3915). The fluorescence intensity of each well was determined
1355
1356 using a plate reader (Perkin-Elmer Victor X2 Multilabel Reader, excitation filter 485 nm, emission
1357
1358 filter 535 nm).
1359
1360

1361
1362 *NLRP ATP-binding and elution experiments-* Approximately 24 h after transient transfection,
1363
1364 HEK293T cell pellets were extracted with 500 μ L of Lysis Buffer. Aliquots of cell lysates (50 μ L)
1365
1366 were incubated with P-linked ATP-Sepharose (50 μ L, to give a 1:1 slurry) at 4 $^{\circ}$ C for 1 h. After
1367
1368 incubation, the ATP-Sepharose was washed 3 times with 1 ml HSWB and then 3 times with 1 mL
1369
1370 LSWB. Various NLRP-GFPs were eluted with increasing ATP or drug candidate solutions from
1371
1372 the resin. Eluates were transferred to a black 96-well plate for fluorescence measurement by a plate
1373
1374 reader (Molecular Devices SpectraMax M2, excitation filter 485 nm, emission filter 535 nm)
1375
1376 and/or were subjected to SDS-PAGE and immunblotting with anti-GFP antibody (Molecular
1377
1378 Probes, Cat# A11122) at a 1:1000 dilution or with anti-NLRP3 antibody (Adipogen, Cat#
1379
1380 AG20B0014) at a 1:1000 dilution. In some cases, blocking experiments were used to assess the
1381
1382 ability of NLRP inhibitors to disrupt binding with ATP Sepharose. Whole cell HEK293T lysates
1383
1384 were pre-incubated with drug (1 h at 5 $^{\circ}$ C) prior to capture of NLRP3 protein with ATP Sepharose
1385
1386 (conditions above). After incubation, the binding reactions were passed through 0.45 μ m
1387
1388 centrifugal spin-filters (Millipore) to separate ATP Sepharose beads from the unbound lysate
1389
1390 fraction.
1391
1392
1393
1394
1395
1396
1397
1398
1399
1400

1401
1402
1403 *NLRP3 inflammasome oligomerization assay-* Full-length NLRP3 was cloned into mammalian
1404 expression plasmids encoding either an N-terminal FLAG tag or a C-terminal GFP tag. Co-
1405 immunoprecipitation assays were completed where oligomerization (under over-expression
1406 conditions in HEK293T cells) could be quantified based on the ability to pull down GFP-tagged
1407 NLRP3 using FLAG-tagged NLRP3. The pull down of GFP-tagged NLRP3 with FLAG-tagged
1408 NLRP3 in the absence of HS203873 treatment served as the positive control, and the results from
1409 the ensuing western blot were expressed as percentages of the positive control via densitometry.
1410
1411 Co-immunoprecipitation experiments using cell lysates from untransfected, GFP-transfected,
1412 NLRP3-GFP alone or FLAG-NLRP3 alone served as negative controls. Each treatment was
1413 conducted in a single 60-mm dish of HEK293T cells transfected with 3 mg of each plasmid using
1414 calcium phosphate and incubated for 48 h post-transfection in the absence or presence of
1415 HS203873.
1416
1417

1418
1419
1420
1421
1422
1423
1424
1425
1426
1427
1428
1429
1430
1431 *NLRP3 ATPase assay-* NLRP3 ATPase activity was determined using the ADP Detection Kit
1432 (MAK033, Sigma Aldrich) according to the manufacturer's instructions. NLRP3-GFP was
1433 expressed in HEK293T cells and purified by immunoprecipitation against the GFP tag. The
1434 ATPase activity was monitored in 96-well microplates with 50 μ L reactions containing 10 μ L of
1435 NLRP3-GFP immunoprecipitate, 25 mM Tris-HCl, pH 7.5, 150 mM NaCl, 10 mM MgCl₂, 0.1
1436 mM ATP in the absence or presence of HS203873 at 37 °C. Some assays used HEK293T cell
1437 lysates with GFP expression as a control.
1438
1439
1440
1441
1442
1443
1444
1445
1446
1447

1448 *Immunoblotting-* Proteins were resolved by SDS-PAGE and transferred to 0.2 μ m polyvinylidene
1449 difluoride (PVDF) membranes with a standard Tris-Glycine transfer buffer containing 10% (v/v)
1450
1451
1452
1453
1454
1455
1456

1457
1458
1459 methanol. The membrane was washed with TBST (25 mM Tris-HCl, 137 mM NaCl, 3 mM KCl,
1460 and 0.05% (v/v) Tween-20). Non-specific binding sites were blocked with 5% (w/v) nonfat dry
1461 milk in TBST. Membranes were washed with TBST and incubated overnight with primary anti-
1462 ASC antibody at a 1:1,000 dilution in 1% (w/v) nonfat dry milk in TBST. Membranes were
1463 incubated for 1 h with HRP-conjugated secondary antibody (dilution 1:5,000) and developed with
1464 enhanced chemiluminescence (ECL) reagent (GE Healthcare, Mississauga, ON). All western blots
1465 were visualized with a LAS4000 Imaging Station (GE Healthcare), ensuring that the representative
1466 signal occurred in the linear range.
1467
1468
1469
1470
1471
1472
1473
1474
1475
1476
1477

1478 *Sample Preparation for SRM-MS-* HEK293T or THP-1 cells were washed with ice-cold PBS,
1479 suspended in 50 mM AMBIC and then lysed by repetitive vortexing and sonication. The cell
1480 lysate was diluted 5-fold with 50 mM AMBIC and then clarified by centrifugation (13,000xg, 10
1481 minutes, 5 °C). The protein concentration was determined by Bradford assay. Protein was reduced
1482 and alkylated by sequential incubation with 5 mM DTT (30 minutes, 50 °C) and 15 mM
1483 iodoacetamide (30 minutes in the dark, ambient temperature). Proteolytic digests were generated
1484 by overnight incubation (37 °C) with trypsin at a ratio of 1:50 (w/w) plus an additional 5 mM DTT.
1485 The resulting tryptic peptides were frozen at -20 °C until SRM-MS analysis.
1486
1487
1488
1489
1490
1491
1492
1493
1494
1495
1496
1497

1498 *SRM-MS Program Design-* Tryptic peptides from NLRP3 were selected using the Global
1499 Proteome Machine Database (GPMDB), ProteinAtlas or from previously published reports. For
1500 bioinformatic verification, peptides were checked using the SRM collider program. The SRM-MS
1501 method was constructed using Skyline and transitions were confirmed bioinformatically and
1502 technically. Some NLRP3 peptides were selected *de novo* in Skyline. Sites of post-translational
1503
1504
1505
1506
1507
1508
1509
1510
1511
1512

1513
1514
1515 modifications were also taken into account in the selection of peptides. For technical verification
1516
1517 and method optimization, NLRP3 peptides were synthesized as well as derived from trypsin-
1518
1519 digested heterologous expressed protein. The final SRM-MS method was scheduled using iRT
1520
1521 within Skyline to define retention time windows of four minutes to ensure at least ten data points
1522
1523 across a peak and less than 100 concurrent transitions.
1524
1525

1526
1527
1528 *HPLC and Mass Spectrometer Instrumentation-* Chromatography was completed using a Dionex
1529
1530 Ultimate 3000 and Chromeleon Express software package with a trap-column under reverse-
1531
1532 elution conditions (OPTI-TRAP MacroColumn-Peptide 50 µl, large capacity, 3 mm x 12 mm;
1533
1534 Optimize Technology, Oregon City, OR). A C18 PepMap precolumn (100 Å pore size, 5 µm
1535
1536 particle size, 5 mm length, 300 µm i.d.; ThermoFisher Scientific) was connected upstream of the
1537
1538 separation column. Tryptic peptides were separated on a PepMap300 C18 column (5 µm particle
1539
1540 size, 300 Å pore size, 1 mm x 150 mm, ThermoFisher Scientific) with a 44-minute gradient from
1541
1542 2% to 40% acetonitrile with 0.1% (v/v) formic acid at a flow rate of 50 µL/min. Eluted peptides
1543
1544 were subjected to in-line electrospray ionization and analyzed with a hybrid triple quadrupole-ion
1545
1546 trap mass spectrometer (QTrap4500 running Analyst software; ABSciex, Framingham, MA).
1547
1548
1549
1550

1551 1552 1553 1554 **ACKNOWLEDGEMENTS** 1555

1556
1557
1558 This work was supported by grants-in-aid from the University of Calgary University Research
1559
1560 Grants Committee, the Canadian National Transplant Research Program (CNTRP), the Canadian
1561
1562 Institutes of Health Research (CIHR) Health Challenges in Chronic Disease Signature Initiative
1563
1564
1565
1566
1567
1568

1569
1570
1571 (#THC-13523), and the Canada Foundation for Innovation. K.-C.L. was supported by a University
1572
1573 of Calgary Eyes-High Fellowship. C.F.S. was supported by a Natural Sciences and Engineering
1574
1575 Research Council (NSERC) Postgraduate Scholarship. D.A.M. was an Alberta Innovates Health
1576
1577 Solutions (AIHS) Clinical Senior Scholar and held a Canada Research Chair in Inflammation and
1578
1579 Kidney Disease. J.A.M. was an AIHS Senior Scholar and held a Marie Curie International
1580
1581 Incoming Fellowship.
1582
1583
1584
1585
1586
1587
1588
1589
1590
1591
1592
1593
1594
1595
1596
1597
1598
1599
1600
1601
1602
1603
1604
1605
1606
1607
1608
1609
1610
1611
1612
1613
1614
1615
1616
1617
1618
1619
1620
1621
1622
1623
1624

1625
1626
1627 **Table 1. SRM-MS screen of NLRP3 for proteotypic peptides.** Human NLRP3 protein
1628 (UniProtKB: Q96P20) was expressed in HEK293T cells (ATCC: CRP-1573). Whole cell lysates
1629 were subjected to tryptic digestion and SRM-MS analyses. The relative SRM-MS signal intensities
1630 of tryptic peptides are indicated with: (+) - robust signal and meets limit-of-detection criteria; (?)
1631 - identification was unclear based on weak signal intensity of transitions, (-) - not detected, and
1632 (n/a) - not examined, outside of dynamic range of mass spectrometer.
1633
1634
1635
1636
1637
1638
1639
1640
1641
1642
1643
1644
1645
1646
1647
1648
1649
1650
1651
1652
1653
1654
1655
1656
1657
1658
1659
1660
1661
1662
1663
1664
1665
1666
1667
1668
1669
1670
1671
1672
1673
1674
1675
1676
1677
1678
1679
1680

1681
1682
1683
1684
1685
1686
1687
1688
1689
1690
1691
1692
1693
1694
1695
1696
1697
1698
1699
1700
1701
1702
1703
1704
1705
1706
1707
1708
1709
1710
1711
1712
1713
1714
1715
1716
1717
1718
1719
1720
1721
1722
1723
1724
1725
1726
1727
1728
1729
1730
1731
1732
1733
1734
1735
1736

NLRP3 Tryptic Peptides	Residue No.	HEK293
K.MHLEDYPPQK.G	[26, 35]	?
K.GCIPLPR.G	[36, 42]	+
K.ADHVDLATLMIDFNGEK.A	[48, 65]	-
K.AWAMAVWIFAAINR.R	[66, 79]	?
K.WGSDNAR.V	[93, 99]	-
R.VSNPTVICQEDSIEEEWMLLEYLSR.I	[100, 125]	n/a
R.FQCIEDR.N	[147, 153]	+
R.LGESVSLNK.R	[157, 165]	?
R.EQELLAIGK.T	[183, 191]	+
K.TCESPVSPIK.M	[194, 203]	+
K.MELLDPDDEHSEPVHTVVFQGAAGIGK.T	[204, 231]	n/a
K.MMLDWASGTLYQDR.F	[238, 251]	+
R.FDYLFYIHC.R.E	[252, 261]	+
R.EVSLVTQR.S	[262, 269]	+
R.SLGDLMSCCPDPNPIHK.I	[270, 288]	-
R.IFLMDGFDLQGAFFDEHIGPLCTDWQK.A	[296, 323]	n/a
R.GDILLSSLIR.K	[327, 336]	+
K.LLPEASLLITRTPVALEK.L	[339, 356]	+
K.LQHLLDHP.R.H	[357, 365]	?
R.HVEILGFSEAK.R	[366, 376]	+
K.YFSDEAQR.A	[384, 392]	+
R.AAFSLIQENEVLFTMCFIPLVCWIVCTGLK.Q	[393, 422]	n/a
K.QQMESGK.S	[423, 429]	-
K.SLAQTSK.T	[430, 436]	?
K.TTTAVYVFFLSSLLQPR.G	[437, 453]	-
R.GGSQEHGLCAHLWGLCSLAADGIWNQK.I	[454, 480]	n/a
K.ILFEESDLR.N	[481, 489]	+
R.NHGLQK.A	[490, 495]	+
K.ADVSAFLR.M	[496, 503]	+
R.MNLFQK.E	[504, 509]	+
K.EVDCEK.F	[510, 515]	-
K.FYSFIHMTFQEFFAAMYLLLEEK.E	[516, 539]	n/a
R.TNVPGSR.L	[543, 549]	-
R.DVTVLLENYGK.F	[556, 566]	+
K.GYLIFVVR.F	[570, 577]	+
R.FLFGLVNQR.T	[578, 587]	+
R.TSYLEK.K	[588, 593]	+
K.ISQQR.L	[599, 604]	-
K.LQIQPSQLELFYCLYEMQEEDFVQR.A	[620, 644]	n/a
R.AMDYFPK.I	[645, 651]	+
K.IEINLSTR.M	[652, 659]	+
R.MDHMVSSFCIENCHR.V	[660, 674]	-
R.VESLSLGFHNMPEK.E	[675, 688]	?
R.HLDMVQCVPSSSHAACSHGLVNSHLTSSFCR.G	[699, 730]	n/a
R.GLFSVLSTSQLTELDLSDNSLGDPMR.V	[731, 758]	n/a
R.VLCETLQHPCNIR.R	[759, 772]	?
R.CGLSHECCFDISLVLSNQK.L	[779, 798]	-
K.LVELDLSDNALGDFGIR.L	[799, 815]	+
R.LLCVGLK.H	[816, 822]	(+)
K.HLLCNLK.K	[823, 829]	(+)
K.LWLVSCCLTSACQDLASVLTSHSLTR.L	[831, 858]	n/a
R.LYVGENALGDSGVAILCEK.A	[859, 877]	+
K.NPQCNLQK.L	[880, 887]	-
R.GNTLGDK.G	[920, 926]	-
K.LLCEGLLHPDCK.L	[930, 941]	-
K.LQVLELDNCLTSHCCWDLSTLLTSSQSLR.K	[942, 971]	n/a
K.LSLGNNDLGDVGMMFCEVLK.Q	[973, 993]	+
K.QQSCLLQNLGLSEMYFNK.S	[994, 1014]	+
K.SALETLQEEKPELTVVFPSW.-	[1015, 1035]	-

Table 2. Anti-inflammatory compounds associated with inhibition of the NLRP3 inflammasome.

Drug	Target	Effective Concentration
Andrographolide	Undefined	30 μ M [83]
α,β -unsaturated carbonyl warheads	NLRP3	10 μ M [92,93]
Bay-11-7082	NLRP3	<15 μ M [88]
	Undefined	10 μ M [90]
	TLR - NF- κ B	30 μ M [84]
Bromoxone	Undefined	1 μ M [84]
C172	Undefined (NLRP3?)	<10 μ M [95]
CRID3	ASC	25-50 μ M [80]
CY-09	NLRP3	<10 μ M [95]
Fc11a-2	Caspase-1 ASC	10 μ M [87]
Glyburide	Undefined (K ⁺ efflux)	50-100 μ M [85]
INF39	NLRP3	10-100 μ M [94]
Isoliquiritigenin	NLRP3	<10 μ M [96]
Luteoloside	Undefined	25-50 μ M [97]
MCC950	NLRP3	0.1 μ M [81]
3,4-methylenedioxy- β -nitrostyrene	NLRP3	<5 μ M [91]
5Z-7-oxozeaenol	TLR - NF- κ B	1 μ M [84]
Parthenolide	Caspase-1 NLRP3	10 μ M [88]
Prostaglandin 15d-PGJ2	Undefined	20 μ M [97]
Sanguinarine	TLR - NF- κ B	5 μ M [84]
TAK-242 (Resatorvid)	TLR - NF- κ B	20 μ M [84]
16673-34-0	Undefined	400 μ M [86]

1793
1794
1795 **FIGURE 1. Immobilized ATP for affinity capture applications.** Various immobilized ATP
1796
1797
1798
1799
1800
1801
1802
1803
1804
1805
1806
1807
1808
1809
1810
1811
1812
1813
1814
1815
1816
1817
1818
1819
1820
1821
1822
1823
1824
1825
1826
1827
1828
1829
1830
1831
1832
1833
1834
1835
1836
1837
1838
1839
1840
1841
1842
1843
1844
1845
1846
1847
1848

FIGURE 1. Immobilized ATP for affinity capture applications. Various immobilized ATP Sepharose matrices can be generated by chemical coupling through: the γ -phosphate group (P-link), the N6- and N8- amino groups of the purine ring of the nucleotide, respectively (N-link) or either of the hydroxyls at the C2 or C3 position of the ribose ring (R-link).

FIGURE 2. Comparison of NLRP3 capture with various ATP Sepharose linkages. Various ATP Sepharose resins were incubated with whole cell lysates obtained from HEK293T cells stably-expressing NLRP3-GFP. ATP Sepharoses included: (A) P-linked (0.25 μ mol ATP/mL resin); (B) N6-linked (5 μ mol ATP/mL resin); (C) N8-linked (5 μ mol ATP/mL resin); (D) R-linked (5 μ mol ATP/mL resin), and (E) cleavable diazo-P-linked (0.25 μ mol ATP/mL resin). Following gentle mixing, the unbound fractions containing proteins that were not successfully captured by the ATP Sepharose were collected and probed for NLRP3 by immunoblotting. NLRP3 binding (%) was calculated from the densitometry data as the [unbound NLRP3 / total NLRP3 input]. Data are representative of three independent experiments using unique whole cell lysates. Bar graphs and error bars represent the mean \pm standard deviation.

FIGURE 3. NLRP3-binding properties with ATP affinity capture chromatography. In (A), plasmids encoding either untagged-NLRP3 or NLRP3-GFP were transfected into HEK293T cells. In (B), PMA-differentiated THP-1 macrophage lysates were combined with P-linked ATP-Sepharose. After incubation with P-linked ATP-Sepharose, charged beads were washed and developed with ATP solutions. Eluted samples were immunoblotted with anti-NLRP3 antibody.

1849
1850
1851 **FIGURE 4. Ligand density influences NLRP3 capture and competitive elution profiles from**
1852 **P-linked ATP Sepharose.** Whole cell lysates obtained from stably-expressing NLRP3-GFP
1853 HEK293T cells were incubated at a 2:1 volumetric ratio with various P-linked ATP Sepharose
1854 resins (increasing ligand densities of 0.1-0.25 $\mu\text{mol ATP/mL}$) with gentle mixing for 1 hour at 4
1855 $^{\circ}\text{C}$. (A) The % capture efficiency was calculated from NLRP3 immunoblot data as the Input
1856 Density - [Unbound Density/Input Density]. CL: cell lysate; FT: flow-through, unbound material.
1857 (B) Following binding and extensive washing, NLRP3-GFP bound ATP Sepharose resin was
1858 evenly distributed to wells of a 96-well filter plates. ATP was added, plates were centrifuged, and
1859 the recovered eluents were probed for NLRP3 by immunoblotting. (C), the % of total eluted
1860 NLRP3 by ATP at each of the individual concentrations was calculated. (D), densitometric data
1861 also highlight differences in elution profiles observed for each ATP concentration. Data are
1862 representative of three independent experiments. Graphs and error bars represent the mean \pm
1863 standard deviation.
1864
1865
1866
1867
1868
1869
1870
1871
1872
1873
1874
1875
1876
1877
1878
1879
1880

1881 **FIGURE 5. Sample processing with immobilized ATP improves SRM-MS analyses of**
1882 **NLRP3.** PMA-differentiated THP-1 cells were treated with nigericin (20 μM ; 45 min). Whole cell
1883 lysates were used to profile signature peptides originating from NLRP3 protein. Four
1884 representative spectra of transitions identified from NLRP3 signature peptides are provided as
1885 examples of improved signal detection with P-linked ATP Sepharose sample processing prior to
1886 SRM-MS analyses. The peptides and their position within the NLRP3 sequence are indicated
1887 above the spectra. Each peptide was identified by its five highest transitions (y- and b-ions), and
1888 the arrow head notes the peak of NLRP3 peptide elution.
1889
1890
1891
1892
1893
1894
1895
1896
1897
1898
1899
1900
1901
1902
1903
1904

1905
1906
1907 **FIGURE 6. NLRP proteins are effectively captured with P-linked ATP Sepharose.** In (A),
1908 HEK293T cells were transfected with various NLRPs-GFP plasmids. Whole cell extracts were
1909 incubated with P-linked ATP Sepharose. After incubation, the ATP Sepharose was washed
1910 extensively, and the various NLRP-GFPs were eluted with the indicated ATP solutions (0 - 300
1911 mM). Fluorescence counts from elution samples were determined using a plate reader (Molecular
1912 Devices SpectraMax M2, excitation filter 485nm, emission filter 535nm). In (B), the binding
1913 efficiency for each NLRP-GFP is expressed as the (Input Fluorescence - Unbound
1914 Fluorescence/Input Fluorescence). In (C), the eluates were further probed for GFP-tagged NLRPs
1915 by immunoblotting with anti-GFP antibody. Data are representative of three independent
1916 experiments. Bar graphs shown represent the mean \pm standard deviation (error bars).
1917
1918
1919
1920
1921
1922
1923
1924
1925
1926
1927
1928
1929
1930

1931 **FIGURE 7. FLECS screening to identify compounds that compete NLRP3 from P-linked**
1932 **ATP Sepharose.** In (A), HEK293T cell lysates containing NLRP3-GFP were incubated with P-
1933 linked ATP Sepharose. After distributing charged beads into 96-well filter plates, drug candidates
1934 or ATP solutions (10-250 mM as positive controls) were applied for competitive elution. Displaced
1935 proteins were collected by centrifugation in catch plates, and the fluorescence in each well was
1936 determined. All wells containing >3000 fluorescence counts were considered potential positive
1937 hits. Eluate from each NLRP3-GFP positive well was validated by immunoblotting. In (B-D), PMA-
1938 differentiated THP-1 cells were primed with LPS (1 ng/mL) and then treated with extracellular
1939 ATP (exATP; 5 mM, 3 h) in the absence or presence of the indicated drug candidates (50 μ M, 2
1940 h), and DMSO was used as a vehicle control. After treatment, the culture supernatants were
1941 analyzed for IL-1 β by ELISA (B). In subsequent studies, HS203873 (indicated concentrations),
1942 glyburide (50 μ M) and Bay 11-7082 (20 μ M) were applied to THP-1 cells. After exposure to
1943
1944
1945
1946
1947
1948
1949
1950
1951
1952
1953
1954
1955
1956
1957
1958
1959
1960

1961
1962
1963
1964
1965
1966
1967
1968
1969
1970
1971
1972
1973
1974
1975
1976
1977
1978
1979
1980
1981
1982
1983
1984
1985
1986
1987
1988
1989
1990
1991
1992
1993
1994
1995
1996
1997
1998
1999
2000
2001
2002
2003
2004
2005
2006
2007
2008
2009
2010
2011
2012
2013
2014
2015
2016

extracellular ATP, the cell supernatants were probed for IL-1 β by ELISA (C) and processed caspase-1 by immunoblotting (D). Chemical structure of HS203873 is provided in (E). Data are representative of n=3 independent experiments. Bar graphs shown represent the mean \pm standard deviation (error bars) of triplicate wells.

FIGURE 8. HS203873 attenuates the ATP-binding, ATP hydrolysis and oligomerization properties of NLRP3. In (A), NLRP3 oligomerization can be generated spontaneously in HEK293T cells with co-incident overexpression of FLAG-NLRP3 and NLRP3-GFP. Immunoprecipitation of NLRP3 inflammasomes from lysates with anti-FLAG reveal heteromultimeric NLRP-GFP:FLAG-NLRP complexes. In (B), HS203873 attenuates NLRP3 oligomerization in a concentration-dependent manner. HEK293T cells were transfected as in (A) and incubated with HS203873 for 48 h. Results (n = 3) are presented as the % change (relative to vehicle control) in NLRP3-GFP/FLAG-NLRP signal ratio as measured by densitometry following immunoprecipitation and western blotting. *-significantly different from vehicle control by ANOVA analysis with Dunnett's *post hoc* test. In (C), *in vitro* ATPase assays were completed with immunoprecipitated NLRP3-GFP in the absence and presence of HS203873 (100 μ M). Results are presented as the % change in the nmoles of ADP produced relative to the vehicle control. Bar graphs represent the mean \pm standard deviation (n=5 independent assays). *-significantly different from vehicle control; p<0.05, Student's t-test. In (D), HEK293T cells were transfected with NLRP3-GFP plasmid. Whole cell lysates were incubated with P-linked ATP Sepharose, and then charged beads were developed with HS203873 (0 – 1 mM) or ATP (200 mM). The elutions were probed for GFP-tagged NLRP3 by immunoblotting. In (E), whole cell HEK293T lysates containing expressed NLRP3-GFP were pre-exposed to HS203873 (0 – 1 mM)

2017
2018
2019
2020
2021
2022
2023
2024
2025
2026
2027
2028
2029
2030
2031
2032
2033
2034
2035
2036
2037
2038
2039
2040
2041
2042
2043
2044
2045
2046
2047
2048
2049
2050
2051
2052
2053
2054
2055
2056
2057
2058
2059
2060
2061
2062
2063
2064
2065
2066
2067
2068
2069
2070
2071
2072

or 200 mM ATP prior to incubation with P-linked ATP Sepharose. NLRP3-GFP was measured in the unbound fraction. Data in **(D)** and **(E)** are representative of two independent replicates.

References

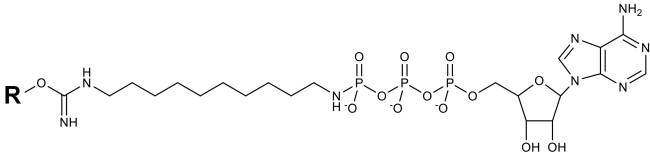
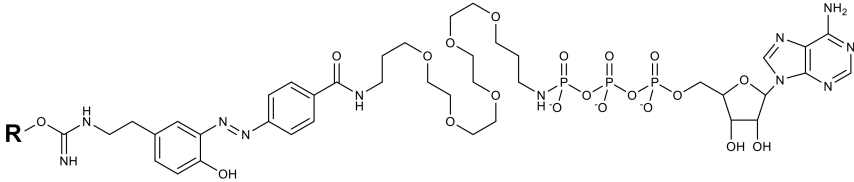
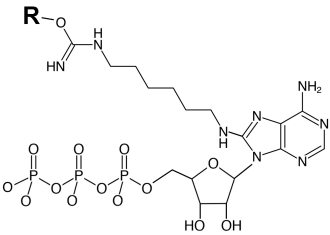
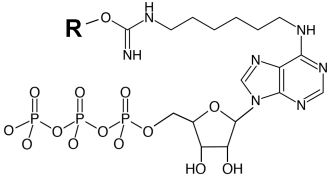
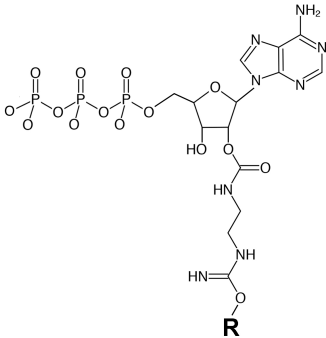
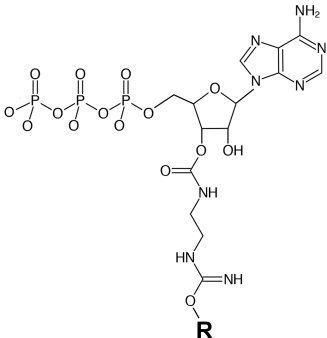
1. Latz, E., T.S. Xiao, and A. Stutz, *Activation and regulation of the inflammasomes*. Nat Rev Immunol, 2013. **13**(6): p. 397-411.
2. Sharma, D. and T.D. Kanneganti, *The cell biology of inflammasomes: Mechanisms of inflammasome activation and regulation*. J Cell Biol, 2016. **213**(6): p. 617-29.
3. Mathur, A., J.A. Hayward, and S.M. Man, *Molecular mechanisms of inflammasome signaling*. J Leukoc Biol, 2018. **103**(2): p. 233-257.
4. Hayward, J.A., et al., *Cytosolic Recognition of Microbes and Pathogens: Inflammasomes in Action*. Microbiol Mol Biol Rev, 2018. **82**(4).
5. Yu, H.B. and B.B. Finlay, *The caspase-1 inflammasome: a pilot of innate immune responses*. Cell Host Microbe, 2008. **4**(3): p. 198-208.
6. Kayagaki, N., et al., *Non-canonical inflammasome activation targets caspase-11*. Nature, 2011. **479**(7371): p. 117-21.
7. Man, S.M., et al., *Salmonella infection induces recruitment of Caspase-8 to the inflammasome to modulate IL-1beta production*. J Immunol, 2013. **191**(10): p. 5239-46.
8. Dinarello, C.A., *Overview of the IL-1 family in innate inflammation and acquired immunity*. Immunol Rev, 2018. **281**(1): p. 8-27.
9. Ting, J.P., et al., *The NLR gene family: a standard nomenclature*. Immunity, 2008. **28**(3): p. 285-7.
10. Lechtenberg, B.C., P.D. Mace, and S.J. Riedl, *Structural mechanisms in NLR inflammasome signaling*. Curr Opin Struct Biol, 2014. **29**: p. 17-25.
11. Manji, G.A., et al., *PYPAF1, a PYRIN-containing Apaf1-like protein that assembles with ASC and regulates activation of NF-kappa B*. J Biol Chem, 2002. **277**(13): p. 11570-5.
12. Srinivasula, S.M., et al., *The PYRIN-CARD protein ASC is an activating adaptor for caspase-1*. J Biol Chem, 2002. **277**(24): p. 21119-22.
13. Duncan, J.A., et al., *Cryopyrin/NALP3 binds ATP/dATP, is an ATPase, and requires ATP binding to mediate inflammatory signaling*. Proc Natl Acad Sci U S A, 2007. **104**(19): p. 8041-6.
14. Mariathasan, S., et al., *Cryopyrin activates the inflammasome in response to toxins and ATP*. Nature, 2006. **440**(7081): p. 228-32.
15. Dostert, C., et al., *Innate immune activation through Nalp3 inflammasome sensing of asbestos and silica*. Science, 2008. **320**(5876): p. 674-7.
16. Hornung, V., et al., *Silica crystals and aluminum salts activate the NALP3 inflammasome through phagosomal destabilization*. Nat Immunol, 2008. **9**(8): p. 847-56.
17. Halle, A., et al., *The NALP3 inflammasome is involved in the innate immune response to amyloid-beta*. Nat Immunol, 2008. **9**(8): p. 857-65.
18. Duewell, P., et al., *NLRP3 inflammasomes are required for atherogenesis and activated by cholesterol crystals*. Nature, 2010. **464**(7293): p. 1357-61.
19. Pan, J., et al., *Fatty acid activates NLRP3 inflammasomes in mouse Kupffer cells through mitochondrial DNA release*. Cell Immunol, 2018. **332**: p. 111-120.
20. Martinon, F., et al., *Gout-associated uric acid crystals activate the NALP3 inflammasome*. Nature, 2006. **440**(7081): p. 237-41.
21. Wang, X., et al., *Structure Activity Relationships of Engineered Nanomaterials in inducing NLRP3 Inflammasome Activation and Chronic Lung Fibrosis*. NanoImpact, 2017. **6**: p. 99-108.

- 2129
2130
2131
2132
2133
2134
2135
2136
2137
2138
2139
2140
2141
2142
2143
2144
2145
2146
2147
2148
2149
2150
2151
2152
2153
2154
2155
2156
2157
2158
2159
2160
2161
2162
2163
2164
2165
2166
2167
2168
2169
2170
2171
2172
2173
2174
2175
2176
2177
2178
2179
2180
2181
2182
2183
2184
22. Ferko, M.A. and I. Catelas, *Effects of metal ions on caspase-1 activation and interleukin-1beta release in murine bone marrow-derived macrophages*. PLoS One, 2018. **13**(8): p. e0199936.
 23. Cruz, C.M., et al., *ATP activates a reactive oxygen species-dependent oxidative stress response and secretion of proinflammatory cytokines in macrophages*. J Biol Chem, 2007. **282**(5): p. 2871-9.
 24. Lee, G.S., et al., *The calcium-sensing receptor regulates the NLRP3 inflammasome through Ca²⁺ and cAMP*. Nature, 2012. **492**(7427): p. 123-7.
 25. Munoz-Planillo, R., et al., *K(+) efflux is the common trigger of NLRP3 inflammasome activation by bacterial toxins and particulate matter*. Immunity, 2013. **38**(6): p. 1142-53.
 26. Pettrilli, V., et al., *Activation of the NALP3 inflammasome is triggered by low intracellular potassium concentration*. Cell Death Differ, 2007. **14**(9): p. 1583-9.
 27. Park, S., et al., *The mitochondrial antiviral protein MAVS associates with NLRP3 and regulates its inflammasome activity*. J Immunol, 2013. **191**(8): p. 4358-66.
 28. Subramanian, N., et al., *The adaptor MAVS promotes NLRP3 mitochondrial localization and inflammasome activation*. Cell, 2013. **153**(2): p. 348-61.
 29. Zhou, R., et al., *A role for mitochondria in NLRP3 inflammasome activation*. Nature, 2011. **469**(7329): p. 221-5.
 30. Hoyt, L.R., et al., *Mitochondrial ROS induced by chronic ethanol exposure promote hyperactivation of the NLRP3 inflammasome*. Redox Biol, 2017. **12**: p. 883-896.
 31. Elliott, E.I., et al., *Cutting Edge: Mitochondrial Assembly of the NLRP3 Inflammasome Complex Is Initiated at Priming*. J Immunol, 2018. **200**(9): p. 3047-3052.
 32. Guo, C., et al., *Bile Acids Control Inflammation and Metabolic Disorder through Inhibition of NLRP3 Inflammasome*. Immunity, 2016. **45**(4): p. 802-816.
 33. Mortimer, L., et al., *NLRP3 inflammasome inhibition is disrupted in a group of auto-inflammatory disease CAPS mutations*. Nat Immunol, 2016. **17**(10): p. 1176-86.
 34. Stutz, A., et al., *NLRP3 inflammasome assembly is regulated by phosphorylation of the pyrin domain*. J Exp Med, 2017. **214**(6): p. 1725-1736.
 35. Juliana, C., et al., *Non-transcriptional priming and deubiquitination regulate NLRP3 inflammasome activation*. J Biol Chem, 2012. **287**(43): p. 36617-22.
 36. Py, B.F., et al., *Deubiquitination of NLRP3 by BRCC3 critically regulates inflammasome activity*. Mol Cell, 2013. **49**(2): p. 331-8.
 37. Kattah, M.G., B.A. Malynn, and A. Ma, *Ubiquitin-Modifying Enzymes and Regulation of the Inflammasome*. J Mol Biol, 2017. **429**(22): p. 3471-3485.
 38. Koonin, E.V. and L. Aravind, *The NACHT family - a new group of predicted NTPases implicated in apoptosis and MHC transcription activation*. Trends Biochem Sci, 2000. **25**(5): p. 223-4.
 39. Leipe, D.D., E.V. Koonin, and L. Aravind, *STAND, a class of P-loop NTPases including animal and plant regulators of programmed cell death: multiple, complex domain architectures, unusual phyletic patterns, and evolution by horizontal gene transfer*. J Mol Biol, 2004. **343**(1): p. 1-28.
 40. Hughes, A.L., *Evolutionary relationships of vertebrate NACHT domain-containing proteins*. Immunogenetics, 2006. **58**(10): p. 785-91.
 41. Danot, O., et al., *Wheel of Life, Wheel of Death: A Mechanistic Insight into Signaling by STAND Proteins*. Structure, 2009. **17**(2): p. 172-82.

- 2185
2186
2187
2188
2189
2190
2191
2192
2193
2194
2195
2196
2197
2198
2199
2200
2201
2202
2203
2204
2205
2206
2207
2208
2209
2210
2211
2212
2213
2214
2215
2216
2217
2218
2219
2220
2221
2222
2223
2224
2225
2226
2227
2228
2229
2230
2231
2232
2233
2234
2235
2236
2237
2238
2239
2240
42. Riedl, S.J., et al., *Structure of the apoptotic protease-activating factor 1 bound to ADP*. Nature, 2005. **434**(7035): p. 926-33.
 43. Proell, M., et al., *The Nod-like receptor (NLR) family: a tale of similarities and differences*. PLoS One, 2008. **3**(4): p. e2119.
 44. MacDonald, J.A., et al., *Biochemical and structural aspects of the ATP-binding domain in inflammasome-forming human NLRP proteins*. IUBMB Life, 2013. **65**(10): p. 851-62.
 45. Radian, A.D., et al., *ATP binding by NLRP7 is required for inflammasome activation in response to bacterial lipopeptides*. Mol Immunol, 2015. **67**(2 Pt B): p. 294-302.
 46. Ye, Z., et al., *ATP binding by monarch-1/NLRP12 is critical for its inhibitory function*. Mol Cell Biol, 2008. **28**(5): p. 1841-50.
 47. Faustin, B., et al., *Reconstituted NALP1 inflammasome reveals two-step mechanism of caspase-1 activation*. Mol Cell, 2007. **25**(5): p. 713-24.
 48. Martino, L., et al., *The Biophysical Characterisation and SAXS Analysis of Human NLRP1 Uncover a New Level of Complexity of NLR Proteins*. PLoS One, 2016. **11**(10): p. e0164662.
 49. Grez, M. and J. Niessing, *Affinity chromatography of poly(A) polymerase on ATP-Sepharose*. FEBS Lett, 1977. **77**(1): p. 57-60.
 50. Haystead, C.M., et al., *Gamma-phosphate-linked ATP-sepharose for the affinity purification of protein kinases. Rapid purification to homogeneity of skeletal muscle mitogen-activated protein kinase kinase*. Eur J Biochem, 1993. **214**(2): p. 459-67.
 51. MacDonald, J.A. and K.B. Storey, *Temperature and phosphate effects on allosteric phenomena of phosphofructokinase from a hibernating ground squirrel (Spermophilus lateralis)*. FEBS J, 2005. **272**(1): p. 120-8.
 52. Moudgil, V.K. and T.E. Eessalu, *Inhibition of nuclear uptake and ATP-Sepharose binding of progesterone-receptor complex by aurintricarboxylic acid*. Arch Biochem Biophys, 1982. **213**(1): p. 98-108.
 53. T'Jampens, D., et al., *Selected BTB/POZ-kelch proteins bind ATP*. FEBS Lett, 2002. **516**(1-3): p. 20-6.
 54. Kikuchi, N., et al., *Molecular shape and ATP binding activity of rat p50, a putative mammalian homologue of RuvB DNA helicase*. J Biochem, 1999. **125**(3): p. 487-94.
 55. Kim, S.Y., et al., *Rapid purification and characterization of nucleoside diphosphate kinase isoforms using ATP-sepharose affinity column chromatography*. Mol Cells, 1997. **7**(5): p. 630-4.
 56. Duncan, J.S., T.A. Haystead, and D.W. Litchfield, *Chemoproteomic characterization of protein kinase inhibitors using immobilized ATP*. Methods Mol Biol, 2012. **795**: p. 119-34.
 57. Hu, Z., et al., *Crystal structure of NLRC4 reveals its autoinhibition mechanism*. Science, 2013. **341**(6142): p. 172-5.
 58. Trayer, I.P. and H.R. Trayer, *Affinity chromatography of nicotinamide nucleotide-dependent dehydrogenases on immobilized nucleotide derivatives*. Biochem J, 1974. **141**(3): p. 775-87.
 59. Boja, E.S. and H. Rodriguez, *Mass spectrometry-based targeted quantitative proteomics: achieving sensitive and reproducible detection of proteins*. Proteomics, 2012. **12**(8): p. 1093-110.
 60. Ebhardt, H.A., et al., *Applications of targeted proteomics in systems biology and translational medicine*. Proteomics, 2015. **15**(18): p. 3193-208.

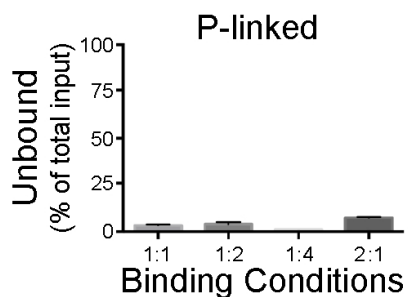
- 2241
2242
2243
2244
2245
2246
2247
2248
2249
2250
2251
2252
2253
2254
2255
2256
2257
2258
2259
2260
2261
2262
2263
2264
2265
2266
2267
2268
2269
2270
2271
2272
2273
2274
2275
2276
2277
2278
2279
2280
2281
2282
2283
2284
2285
2286
2287
2288
2289
2290
2291
2292
2293
2294
2295
2296
61. Gillette, M.A. and S.A. Carr, *Quantitative analysis of peptides and proteins in biomedicine by targeted mass spectrometry*. Nat Methods, 2013. **10**(1): p. 28-34.
 62. Craig, R., et al., *Using annotated peptide mass spectrum libraries for protein identification*. J Proteome Res, 2006. **5**(8): p. 1843-9.
 63. Uhlen, M., et al., *Proteomics. Tissue-based map of the human proteome*. Science, 2015. **347**(6220): p. 1260419.
 64. Craig, R., J.P. Cortens, and R.C. Beavis, *The use of proteotypic peptide libraries for protein identification*. Rapid Commun Mass Spectrom, 2005. **19**(13): p. 1844-50.
 65. Pino, L.K., et al., *The Skyline ecosystem: Informatics for quantitative mass spectrometry proteomics*. Mass Spectrom Rev, 2017.
 66. Rost, H., L. Malmstrom, and R. Aebersold, *A computational tool to detect and avoid redundancy in selected reaction monitoring*. Mol Cell Proteomics, 2012. **11**(8): p. 540-9.
 67. Craig, R., J.P. Cortens, and R.C. Beavis, *Open source system for analyzing, validating, and storing protein identification data*. J Proteome Res, 2004. **3**(6): p. 1234-42.
 68. Liu, X., et al., *Mapping the human plasma proteome by SCX-LC-IMS-MS*. J Am Soc Mass Spectrom, 2007. **18**(7): p. 1249-64.
 69. Carlson, D.A., et al., *Fluorescence linked enzyme chemoproteomic strategy for discovery of a potent and selective DAPK1 and ZIPK inhibitor*. ACS Chem Biol, 2013. **8**(12): p. 2715-23.
 70. Fadden, P., et al., *Application of chemoproteomics to drug discovery: identification of a clinical candidate targeting hsp90*. Chem Biol, 2010. **17**(7): p. 686-94.
 71. Graves, P.R., et al., *Discovery of novel targets of quinoline drugs in the human purine binding proteome*. Mol Pharmacol, 2002. **62**(6): p. 1364-72.
 72. Howe, M.K., et al., *Identification of an allosteric small-molecule inhibitor selective for the inducible form of heat shock protein 70*. Chem Biol, 2014. **21**(12): p. 1648-59.
 73. Kulkarni, M.M., et al., *Cellular fatty acid synthase is required for late stages of HIV-1 replication*. Retrovirology, 2017. **14**(1): p. 45.
 74. Haystead, T.A., *The purinome, a complex mix of drug and toxicity targets*. Curr Top Med Chem, 2006. **6**(11): p. 1117-27.
 75. Zhang, J.H., T.D. Chung, and K.R. Oldenburg, *A Simple Statistical Parameter for Use in Evaluation and Validation of High Throughput Screening Assays*. J Biomol Screen, 1999. **4**(2): p. 67-73.
 76. Guo, H., J.B. Callaway, and J.P. Ting, *Inflammasomes: mechanism of action, role in disease, and therapeutics*. Nat Med, 2015. **21**(7): p. 677-87.
 77. Martinon, F., K. Burns, and J. Tschopp, *The inflammasome: a molecular platform triggering activation of inflammatory caspases and processing of proIL-beta*. Mol Cell, 2002. **10**(2): p. 417-26.
 78. Perregaux, D.G., et al., *Identification and characterization of a novel class of interleukin-1 post-translational processing inhibitors*. J Pharmacol Exp Ther, 2001. **299**(1): p. 187-97.
 79. Laliberte, R.E., et al., *Glutathione s-transferase omega 1-1 is a target of cytokine release inhibitory drugs and may be responsible for their effect on interleukin-1beta posttranslational processing*. J Biol Chem, 2003. **278**(19): p. 16567-78.
 80. Coll, R.C., et al., *The cytokine release inhibitory drug CRID3 targets ASC oligomerisation in the NLRP3 and AIM2 inflammasomes*. PLoS One, 2011. **6**(12): p. e29539.
 81. Coll, R.C., et al., *A small-molecule inhibitor of the NLRP3 inflammasome for the treatment of inflammatory diseases*. Nat Med, 2015. **21**(3): p. 248-55.

- 2297
2298
2299
2300
2301
2302
2303
2304
2305
2306
2307
2308
2309
2310
2311
2312
2313
2314
2315
2316
2317
2318
2319
2320
2321
2322
2323
2324
2325
2326
2327
2328
2329
2330
2331
2332
2333
2334
2335
2336
2337
2338
2339
2340
2341
2342
2343
2344
2345
2346
2347
2348
2349
2350
2351
2352
82. Fan, S.H., et al., *Luteoloside suppresses proliferation and metastasis of hepatocellular carcinoma cells by inhibition of NLRP3 inflammasome*. PLoS One, 2014. **9**(2): p. e89961.
 83. Guo, W., et al., *Small molecule-driven mitophagy-mediated NLRP3 inflammasome inhibition is responsible for the prevention of colitis-associated cancer*. Autophagy, 2014. **10**(6): p. 972-85.
 84. Gong, Y.N., et al., *Chemical probing reveals insights into the signaling mechanism of inflammasome activation*. Cell Res, 2010. **20**(12): p. 1289-305.
 85. Lamkanfi, M., et al., *Glyburide inhibits the Cryopyrin/Nalp3 inflammasome*. J Cell Biol, 2009. **187**(1): p. 61-70.
 86. Marchetti, C., et al., *A novel pharmacologic inhibitor of the NLRP3 inflammasome limits myocardial injury after ischemia-reperfusion in the mouse*. J Cardiovasc Pharmacol, 2014. **63**(4): p. 316-22.
 87. Liu, W., et al., *A novel benzo[d]imidazole derivate prevents the development of dextran sulfate sodium-induced murine experimental colitis via inhibition of NLRP3 inflammasome*. Biochem Pharmacol, 2013. **85**(10): p. 1504-12.
 88. Juliana, C., et al., *Anti-inflammatory compounds parthenolide and Bay 11-7082 are direct inhibitors of the inflammasome*. J Biol Chem, 2010. **285**(13): p. 9792-802.
 89. Rodgers, M.A., et al., *The linear ubiquitin assembly complex (LUBAC) is essential for NLRP3 inflammasome activation*. J Exp Med, 2014. **211**(7): p. 1333-47.
 90. Strickson, S., et al., *The anti-inflammatory drug BAY 11-7082 suppresses the MyD88-dependent signalling network by targeting the ubiquitin system*. Biochem J, 2013. **451**(3): p. 427-37.
 91. He, Y., et al., *3,4-methylenedioxy-beta-nitrostyrene inhibits NLRP3 inflammasome activation by blocking assembly of the inflammasome*. J Biol Chem, 2014. **289**(2): p. 1142-50.
 92. Cocco, M., et al., *Electrophilic warhead-based design of compounds preventing NLRP3 inflammasome-dependent pyroptosis*. J Med Chem, 2014. **57**(24): p. 10366-82.
 93. Cocco, M., et al., *Design, Synthesis, and Evaluation of Acrylamide Derivatives as Direct NLRP3 Inflammasome Inhibitors*. ChemMedChem, 2016. **11**(16): p. 1790-803.
 94. Cocco, M., et al., *Development of an Acrylate Derivative Targeting the NLRP3 Inflammasome for the Treatment of Inflammatory Bowel Disease*. J Med Chem, 2017. **60**(9): p. 3656-3671.
 95. Jiang, H., et al., *Identification of a selective and direct NLRP3 inhibitor to treat inflammatory disorders*. J Exp Med, 2017. **214**(11): p. 3219-3238.
 96. Honda, H., et al., *Isoliquiritigenin is a potent inhibitor of NLRP3 inflammasome activation and diet-induced adipose tissue inflammation*. J Leukoc Biol, 2014. **96**(6): p. 1087-100.
 97. Maier, N.K., S.H. Leppla, and M. Moayeri, *The cyclopentenone prostaglandin 15d-PGJ2 inhibits the NLRP1 and NLRP3 inflammasomes*. J Immunol, 2015. **194**(6): p. 2776-85.
 98. Hughes, P.F., J.J. Barrott, D.A. Carlson, D.R. Loiselle, B.L. Speer, K. Bodoor, L.A. Rund, and T.A.J. Haystead, *A highly selective Hsp90 affinity chromatography resin with a cleavable linker*. Bioorg Med Chem, 2012. **20**(10), 3298-305.
 99. Haneklaus, M., J.D. O'Neil, A.R. Clark, S.L. Masters, and L.A.J. O'Neill, *The RNA-binding protein tristetrarolin (TTP) is a critical negative regulator of the NLRP3 inflammasome*. J Biol Chem, 2017. **292**(17), 6869-881.
 100. Boucher, D., et al., *Caspase-1 self-cleavage is an intrinsic mechanism to terminate inflammasome activity*. J Exp Med, 2018. **215**(3), 827-40.

LINKAGE	IMMOBILIZED ATP STRUCTURE
P-linked	<div style="text-align: center;">  <p>γ-aminodecyl-ATP (C10-spacer)</p> </div> <div style="text-align: center;">  <p>Cleavable diazo-linked ATP</p> </div>
N-linked	<div style="display: flex; justify-content: space-around;"> <div style="text-align: center;">  <p>8-amino-hexyl-ATP N8, C6 spacer</p> </div> <div style="text-align: center;">  <p>6-amino-hexyl-ATP N6, C6 spacer</p> </div> </div>
R-linked	<div style="display: flex; justify-content: space-around;"> <div style="text-align: center;">  </div> <div style="text-align: center;">  </div> </div> <p style="text-align: center;">2'/3'-aminoethyl-carbamoyl-ATP</p>

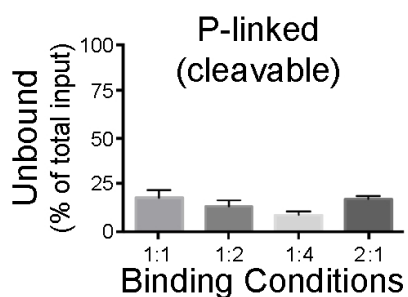
Cell Lysate : Sepharose

1:1 1:2 1:4 2:1 Input



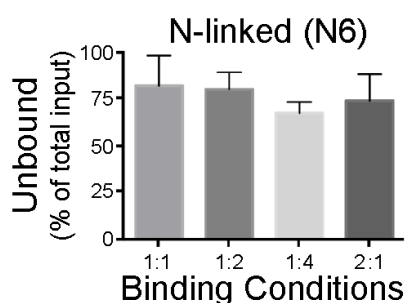
Cell Lysate : Sepharose

1:1 1:2 1:4 2:1 Input



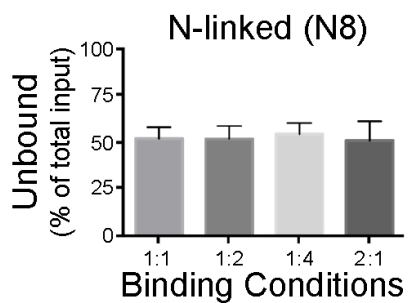
Cell Lysate : Sepharose

1:1 1:2 1:4 2:1 Input



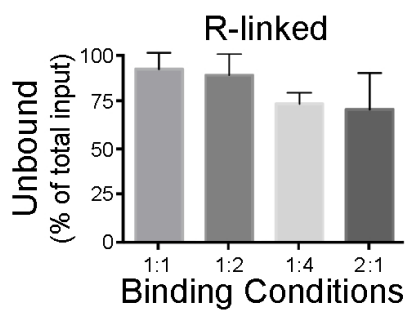
Cell Lysate : Sepharose

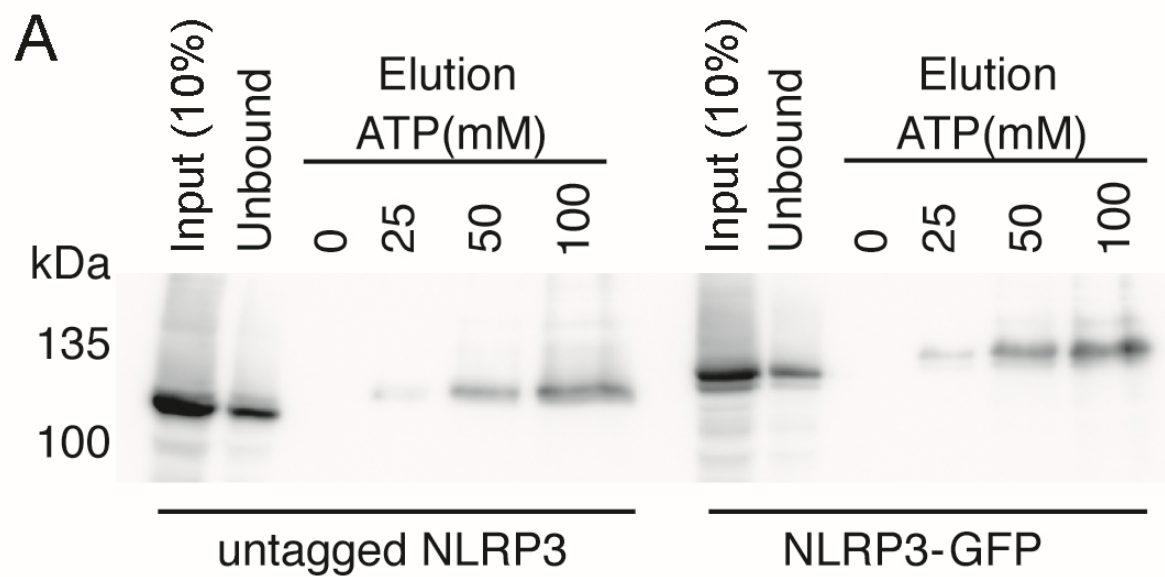
1:1 1:2 1:4 2:1 Input

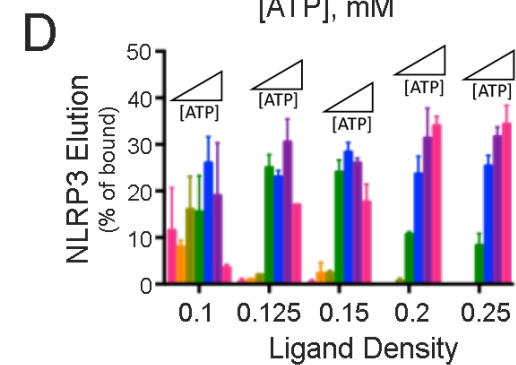
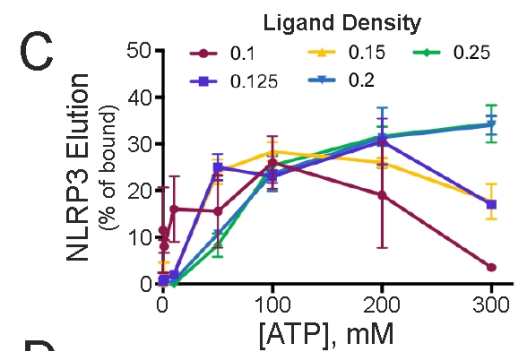
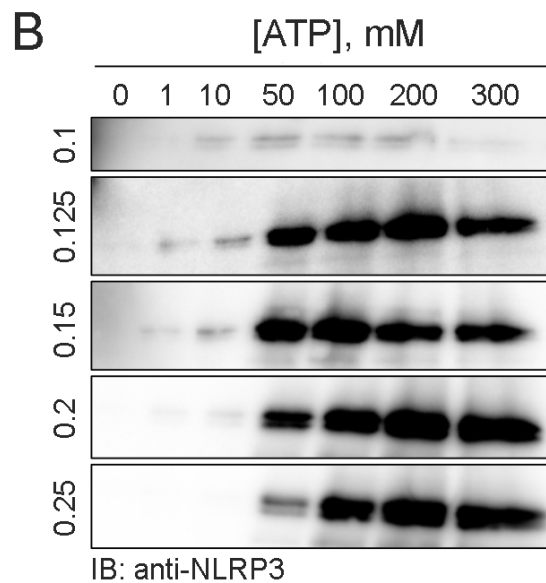
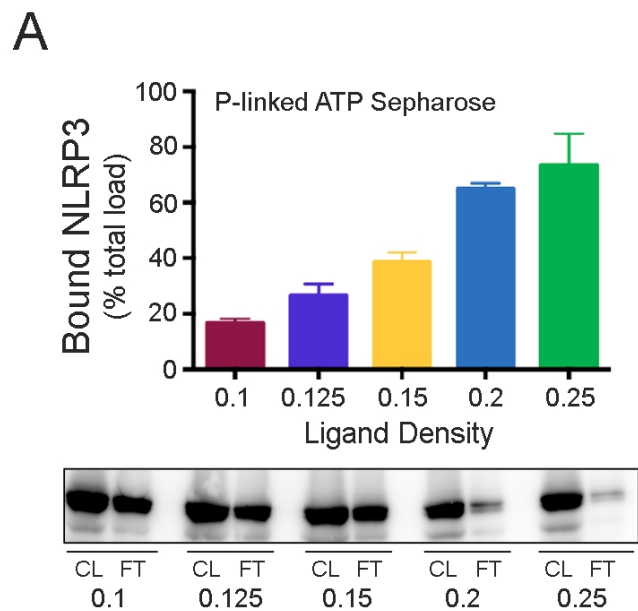


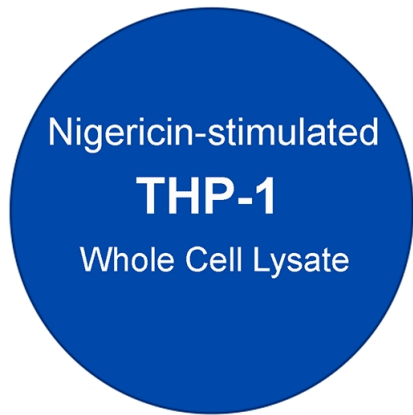
Cell Lysate : Sepharose

1:1 1:2 1:4 2:1 Input





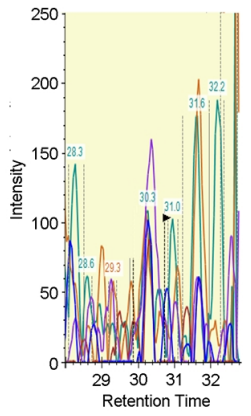




Trypsin
SRM-MS

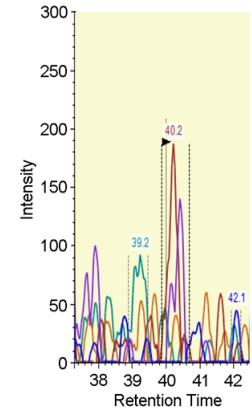
R.EQELLAIGK.T
[183, 191]

y7: 743.486+ y4: 388.255+
y2: 204.134+ b2-18: 240.098+
b3 - 18: 369.141+



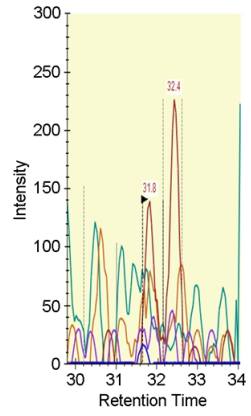
R.GDILLSSLIR.K
[327, 336]

y7: 801.519+ y6: 688.435+
y5: 575.351+ b3: 286.140+
b4: 399.223+



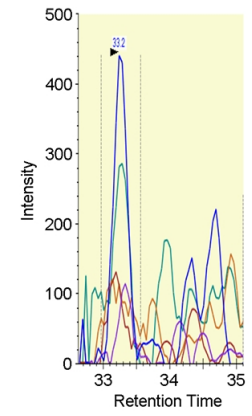
K.ILFEESDLR.N
[481, 489]

y7: 807.436+ y6: 692.409+
y5: 593.341+ y4: 506.309+
b3: 286.140+

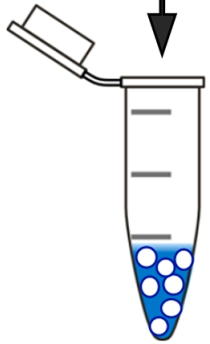


K.ADVSAFLR.M
[496, 503]

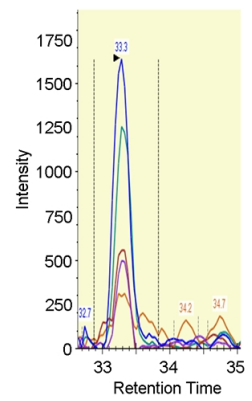
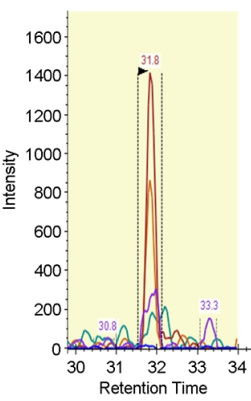
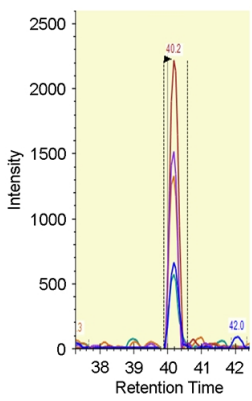
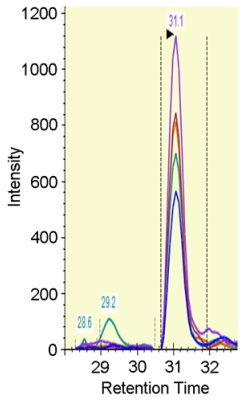
y7: 895.416+ y6: 748.347+
y5: 619.305+ y4: 490.262+
b2: 227.175

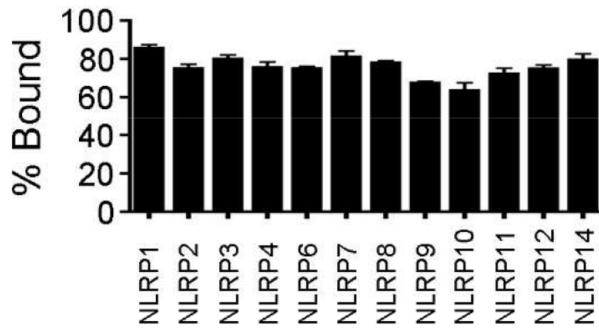
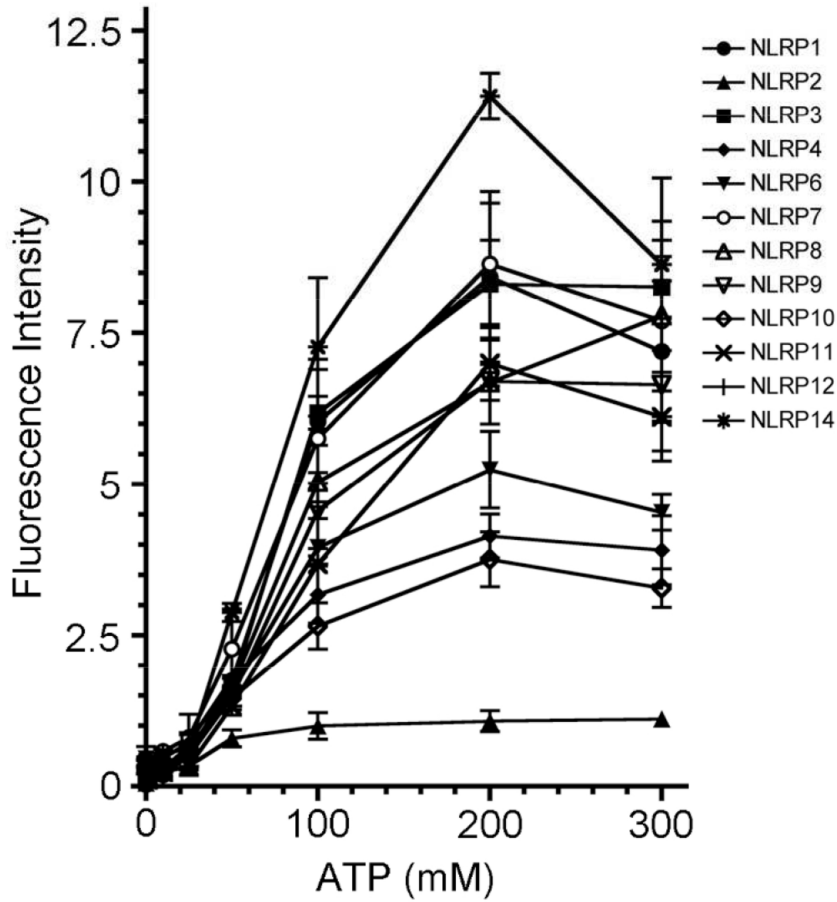
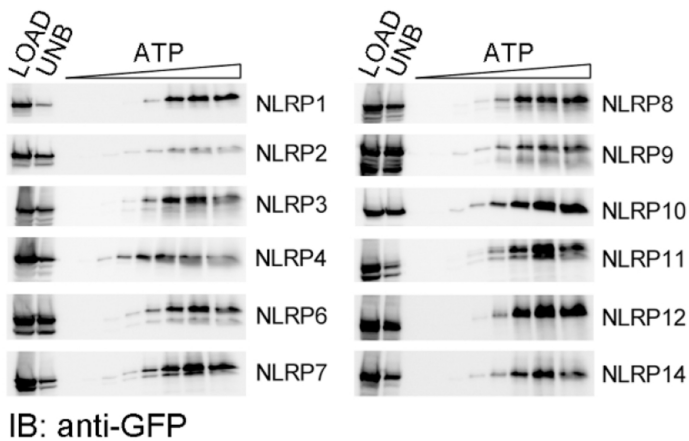


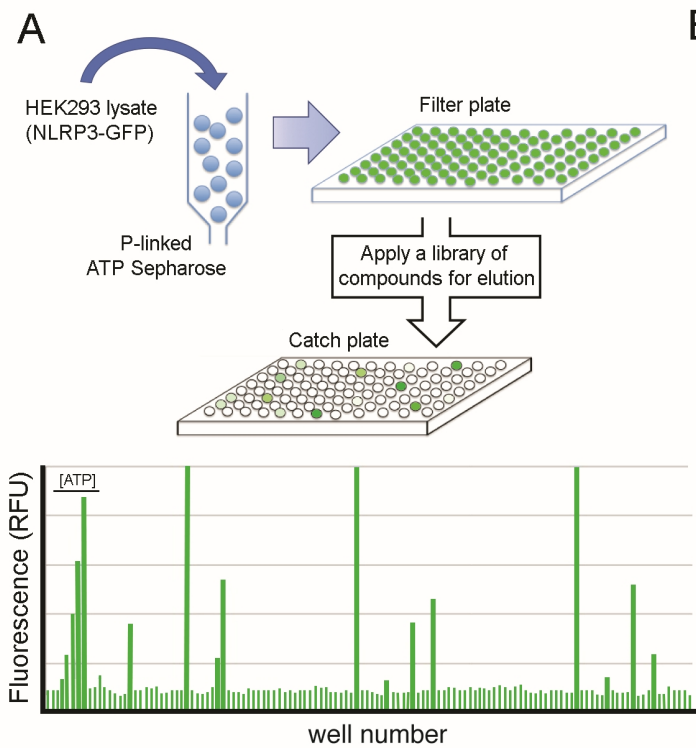
Affinity Capture
P-linked ATP Sepharose



ATP elute & Trypsin
SRM-MS



A**B****C**

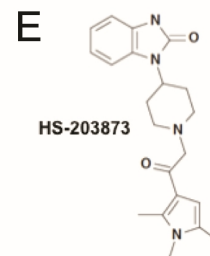
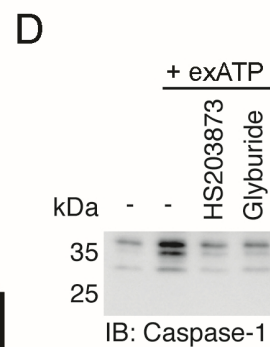
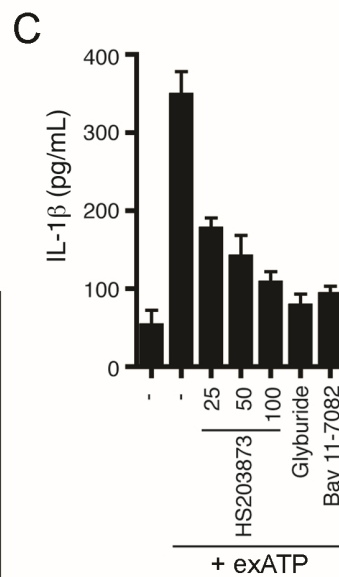
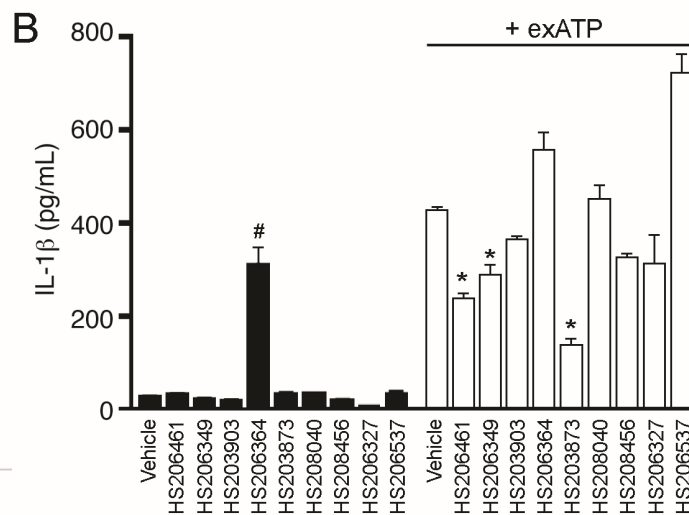


FLECS Screen of NLRP3 Competitors

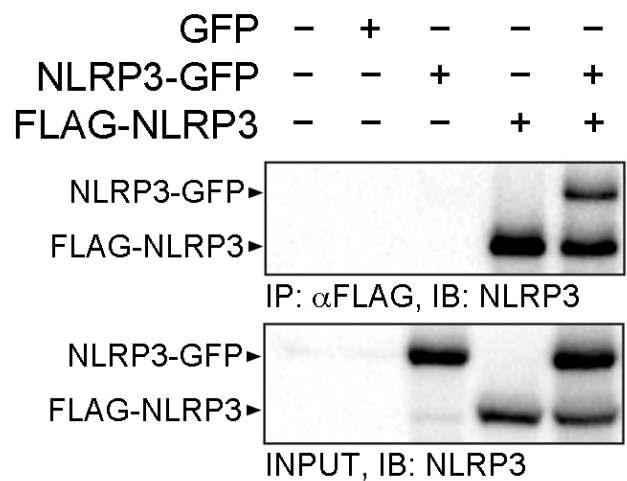
Library of Small Molecules (~3,400 compounds)

~120 positive hits (3.5%) by fluorescence

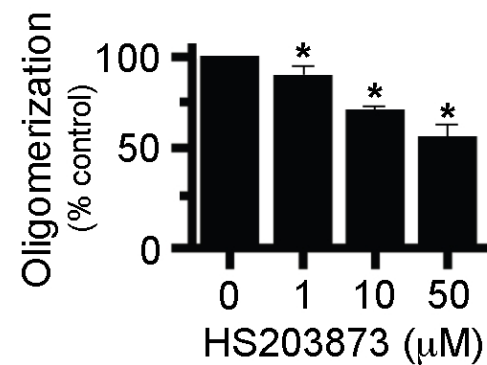
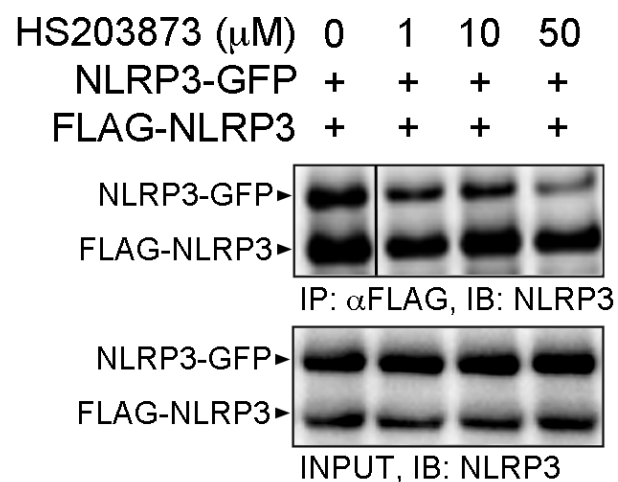
9 confirmed hits (0.26%) by immunoblotting analysis



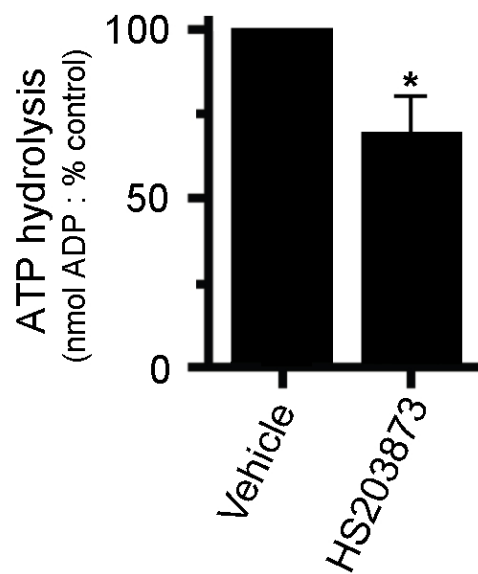
A



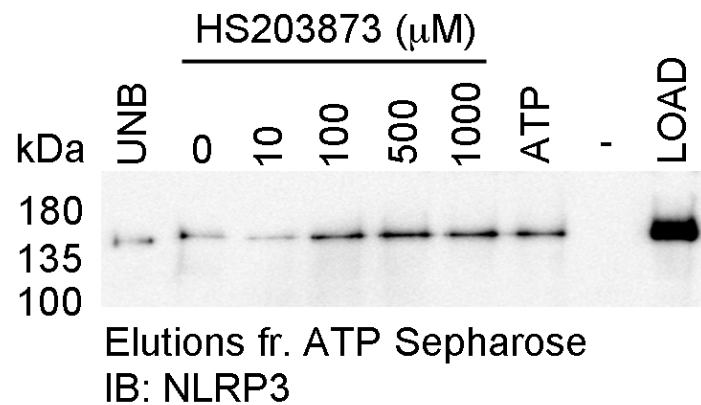
B



C



D



E

